Meteorological Model Performance for Annual 2017 Simulation WRF v3.8

EPA-454/R-22-006

September 2022

Meteorological Model Performance for Annual 2017 Simulation WRF v3.8

U.S. Environmental Protection Agency

Office of Air Quality Planning and Standards

Air Quality Assessment Division

Research Triangle Park, NC

Meteorological Model Performance for Annual 2017 Simulation WRF v3.8

1. INTRODUCTION

The Weather Research and Forecasting model (WRF) was applied for the entire year of 2017 to generate meteorological data to support emissions and photochemical modeling applications for this year. The WRF meteorological fields will be converted to air quality modeling input data and used to support assessments of ozone, PM2.5, visibility, and a variety of toxics.

The WRF model was applied to the 12 km continental United States (12US) scale domain, initialized directly from meteorological analysis data. Model parameterizations and options outlined in this document were chosen based on a series of sensitivity runs performed by U.S. Environmental Protection Agency (USEPA) Office of Research and Development that provided an optimal configuration based on temperature, mixing ratio, and wind field. All WRF simulations were done by CSRA under contract to the USEPA.

2. MODEL CONFIGURATION

Version 3.8 of the WRF model, Advanced Research WRF (ARW) core (Skamarock, 2008) was used for generating the 2017 simulation. Selected physics options include Pleim-Xiu land surface model, Asymmetric Convective Model version 2 planetary boundary layer scheme, Kain-Fritsch cumulus parameterization utilizing the moisture-advection trigger (Ma and Tan, 2009), Morrison double moment microphysics, and RRTMG longwave and shortwave radiation schemes (Gilliam and Pleim, 2010).

The 12US WRF model was initialized using the 12km North American Model (12NAM) analysis product provided by National Climatic Data Center (NCDC). Where 12NAM data was unavailable, the 40km Eta Data Assimilation System (EDAS) analysis (ds609.2) from the National Center for Atmospheric Research (NCAR) was used. Analysis nudging for temperature, wind, and moisture was applied above the boundary layer only. The model simulations were conducted continuously. The 'ipxwrf' program was used to initialize deep soil moisture at the start of the run using a 10-day spinup period (Gilliam and Pleim, 2010). Landuse and land cover data were based on the 2011 National Land Cover Database (NLCD 2011). Sea surface temperatures were ingested from the Group for High Resolution Sea Surface Temperatures (GHRSST) (Stammer et al., 2003) 1km SST data.

Additionally, lightning data assimilation was utilized to suppress (force) deep convection where lightning is absent (present) in observational data. This method is described by Heath et al. (2016) and was employed to help improve precipitation estimates generated by the model.

Figures 2.1 shows the 12US domain, which utilized a Lambert conformal projection centered at (-97,40) with true latitudes of 33 and 45 degrees north. The 12US domain contains 412 cells in the X direction and 372 cells in the Y direction. The atmosphere is resolved with 35 vertical layers up to 50 mb (see table 2.1), with the thinnest layers being nearest the surface to better resolve the planetary boundary layer (PBL).

WRF Layer	**Height (m)**	**Pressure (mb)**	**Sigma**
35	17,556	5000	0.000
34	14,780	9750	0.050
33	12,822	14500	0.100
32	11,282	19250	0.150
31	10,002	24000	0.200
30	8,901	28750	0.250
29	7,932	33500	0.300
28	7,064	38250	0.350
27	6,275	43000	0.400
26	5,553	47750	0.450
25	4,885	52500	0.500
24	4,264	57250	0.550
23	3,683	62000	0.600
22	3,136	66750	0.650
21	2,619	71500	0.700
20	2,226	75300	0.740
19	1,941	78150	0.770
18	1,665	81000	0.800
17	1,485	82900	0.820
16	1,308	84800	0.840
15	1,134	86700	0.860
14	964	88600	0.880
13	797	90500	0.900
12	714	91450	0.910
11	632	92400	0.920
10	551	93350	0.930
9	470	94300	0.940
8	390	95250	0.950
7	311	96200	0.960
6	232	97150	0.970
5	154	98100	0.980
4	115	98575	0.985
3	77	99050	0.990
2	38	99525	0.995
1	19	99763	0.9975
Surface	0	100000	1.000

Table 2.1 WRF layers and their approximate height above ground level.

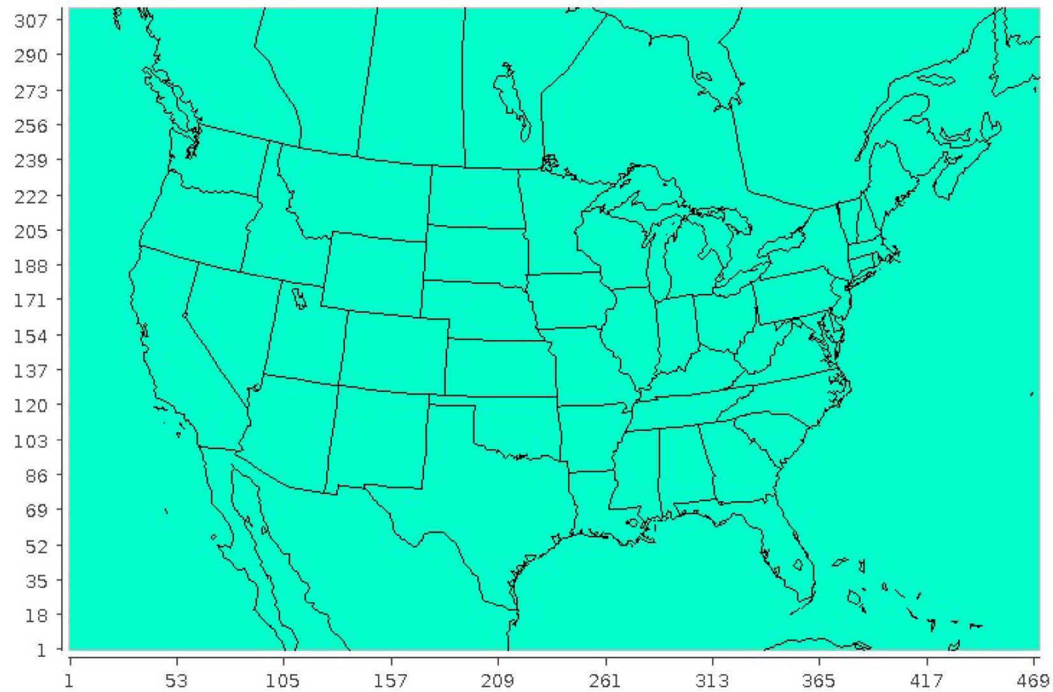

Figure 2.1 Map of WRF model domain: 12US.

3 MODEL PERFORMANCE DESCRIPTION

The WRF model simulations were evaluated to determine whether the output fields represent a reasonable approximation of the actual meteorology that occurred during the modeling period. Identifying and quantifying these output fields allows for a downstream assessment of how the air quality modeling results are impacted by the meteorological data. For the purposes of this assessment, 2-meter temperature and mixing ratio, 10-meter wind speed and direction, and shortwave radiation are quantitatively evaluated. A qualitative and quantitative evaluation of precipitation is also provided.

The observation database for surface-based temperature, wind speed and direction, and mixing ratio is based on measurements made at United States (i.e., National Weather Service) and Canadian (i.e., Environment Canada) airports. The observational dataset (ds472 network) is available from NCAR. Monitors used for evaluation are shown in Figure 3.1.

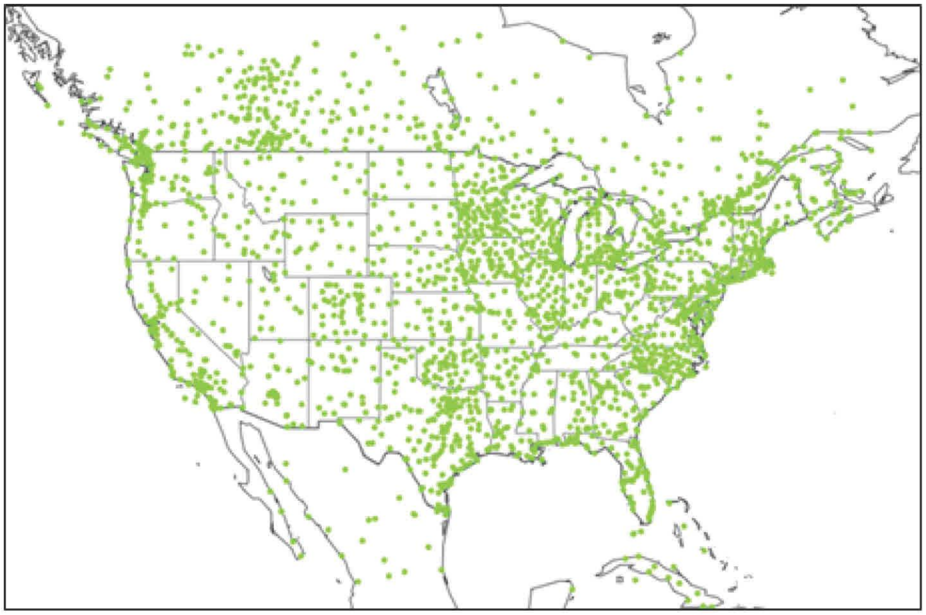

Figure 3.1 Stations used for model performance: ds472 network.

Shortwave downward radiation measurements are taken at Surface Radiation Budget Network (SURFRAD) (https://www.esrl.noaa.gov/gmd/grad/surfrad/index.html) and SOLRAD (formerly ISIS) (https://www.esrl.noaa.gov/gmd/grad/solrad/index.html) monitor locations. The SURFRAD network consists of 7 sites and the SOLRAD network consists of 9 sites across the United States (see Figure 3.2). Both networks are operated by the National Oceanic and Atmospheric Administration (NOAA), with SURFRAD sites existing as a subset of SOLRAD monitors that provide higher level radiation information not used in this evaluation.

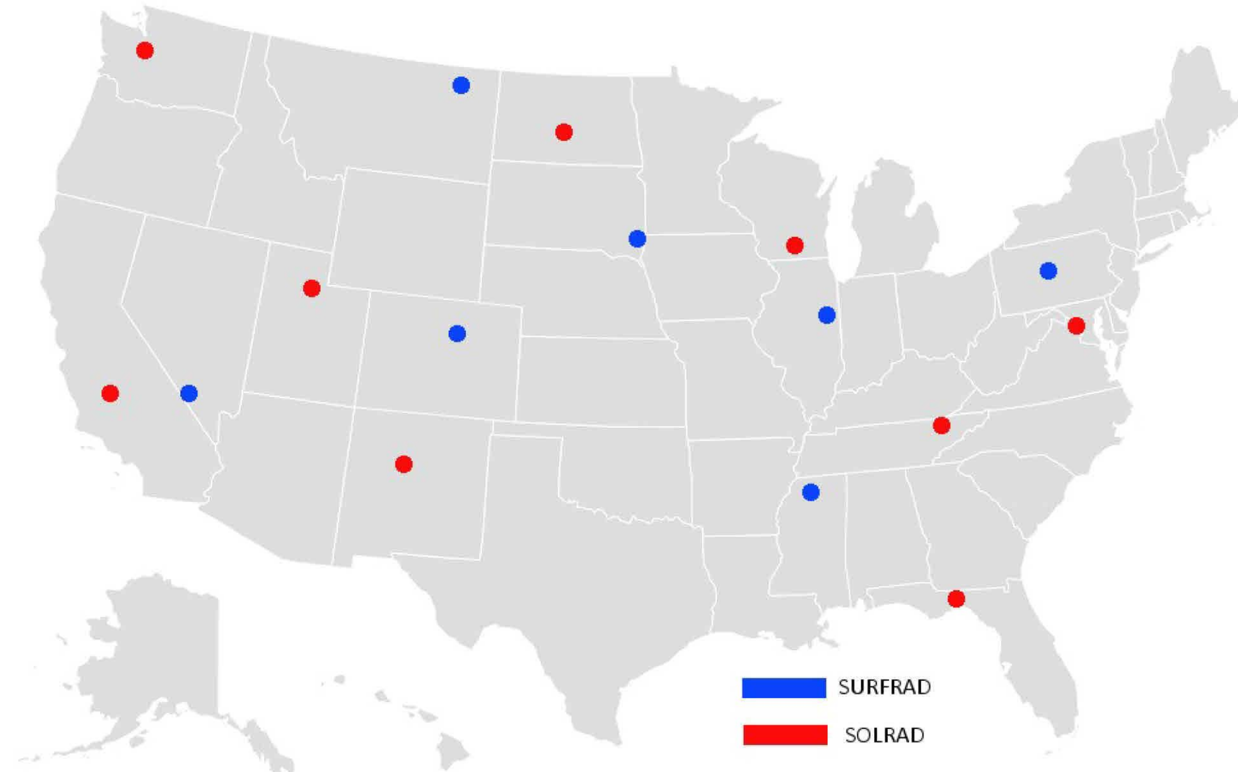

Figure 3.2. Location of SOLRAD and SURFRAD radiation monitors.

Rainfall amounts are estimated by the Parameter-elevation Relationships on Independent Slopes Model (PRISM) model, which uses an elevation-based regression model to analyze precipitation. PRISM's horizontal resolution is approximately 2 to 4 km and is re-projected to the WRF modeling domain for direct comparison to model estimates. The rainfall analysis is limited to the contiguous United States as the model utilizes elevation and measured precipitation data at automated weather stations.

Model performance (i.e., temperature, wind speed, and mixing ratio) is described using quantitative metrics: mean bias, mean (gross) error, fractional bias, and fractional error (Boylan and Russell, 2006). These metrics are useful because they describe model performance in the measured units of the meteorological variable and as a normalized percentage. Since wind direction is reported in compass degrees, estimating performance metrics for wind direction is problematic as modeled and observed northerly winds may be similar but differences would result in a very large artificial bias. For example, the absolute difference in a northerly wind direction measured in compass degrees of 1° and 359° is 358° when the actual difference is only 2°. To address this issue, wind field displacement, or the difference in the U and V vectors between modeled (M) and observed (O) values, is used to assess wind vector performance (Equation 1). Performance is best when these metrics approach 0.

(1) Wind displacement (km) = $(\mathbf{U}_M - \mathbf{U}_O + \mathbf{V}_M - \mathbf{V}_O)$*(1 km/1000 m)*(3600 s/hr)*(1 hr)

Rainfall performance is examined spatially using side-by-side comparisons of monthly total rainfall plots. The WRF model outputs predictions approximately 15 meters above the surface while observations are at 10 meters. WRF generates output at near instantaneous values (90 second time step) as opposed to longer averaging times taken at monitor stations. This should be considered when interpreting model performance metrics.

3.1 Model Performance for Winds

WRF-predicted wind speed estimates are compared to surface-based measurements made in the ds472 network described earlier and shown below in Figure 3.1.1. Regional analysis of statistical metrics for wind speed performance by quarter[1] is shown in Table 3.1.1.

WRF tends to slightly overpredict wind speeds in the early morning and afternoon hours, while slightly underpredicting wind speeds in the late evening and overnight hours. There is no significant seasonal variability noted in terms of wind speed.

The monthly spatial distributions of the wind speed biases (m/s) for all hours (Figures 3.1.2-3.1.5) are presented. In general, WRF slightly overpredicts (0.25 to 0.5 m/s) across much of the eastern US. Conversely, WRF tends to underpredict (-0.25 to -1 m/s) wind speeds in the western US, which persists across much of the year. As noted above, these biases generally persist regardless of changes in season.

[1] Quarters are Q1 (January, February, March), Q2 (April, May, June), Q3 (July, August, September), and Q4 (October, November, December).

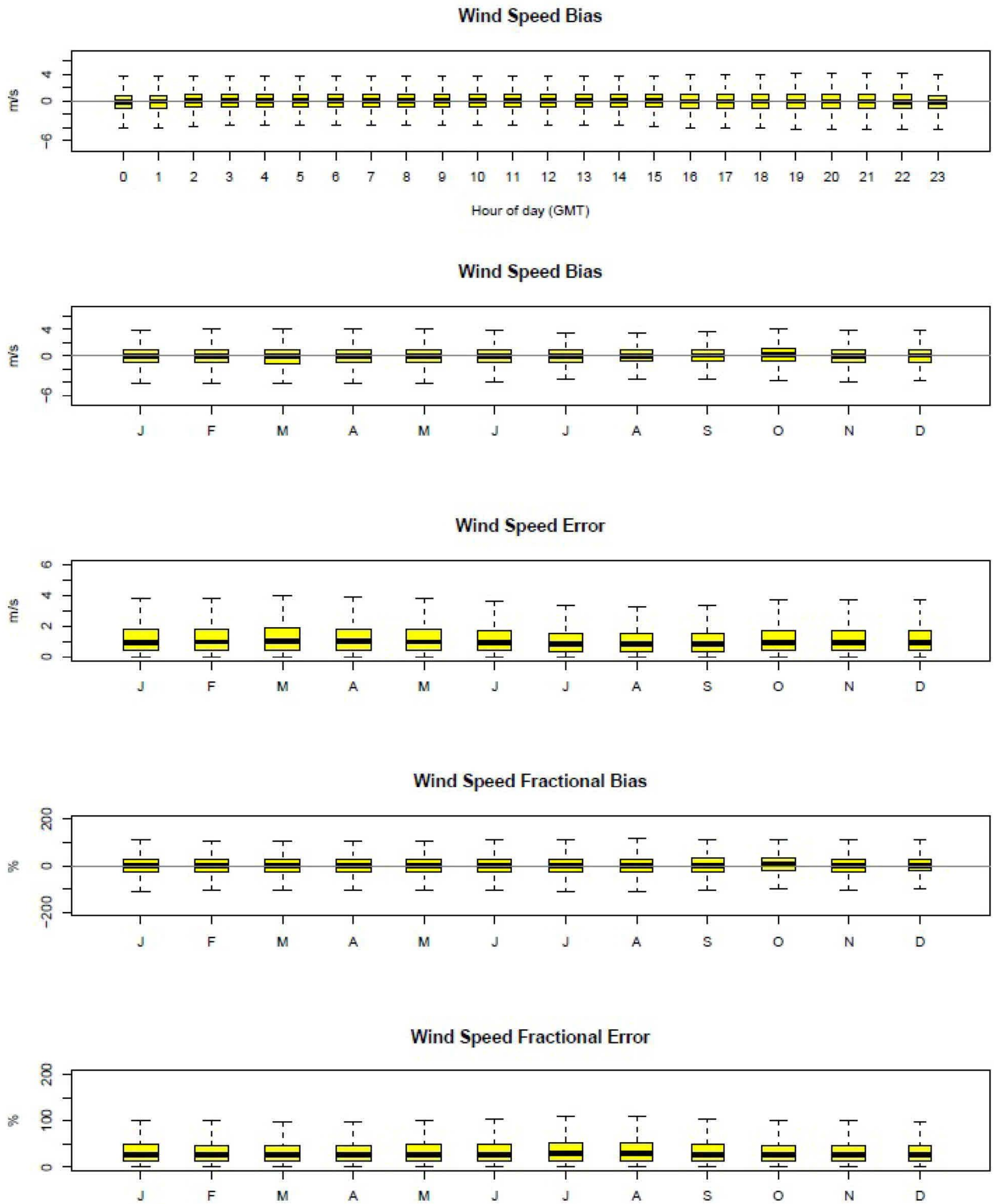

Figure 3.1.1. Distribution of hourly bias by hour and hourly bias, error, fractional bias, and fractional error for wind speed by month for 12US domain.

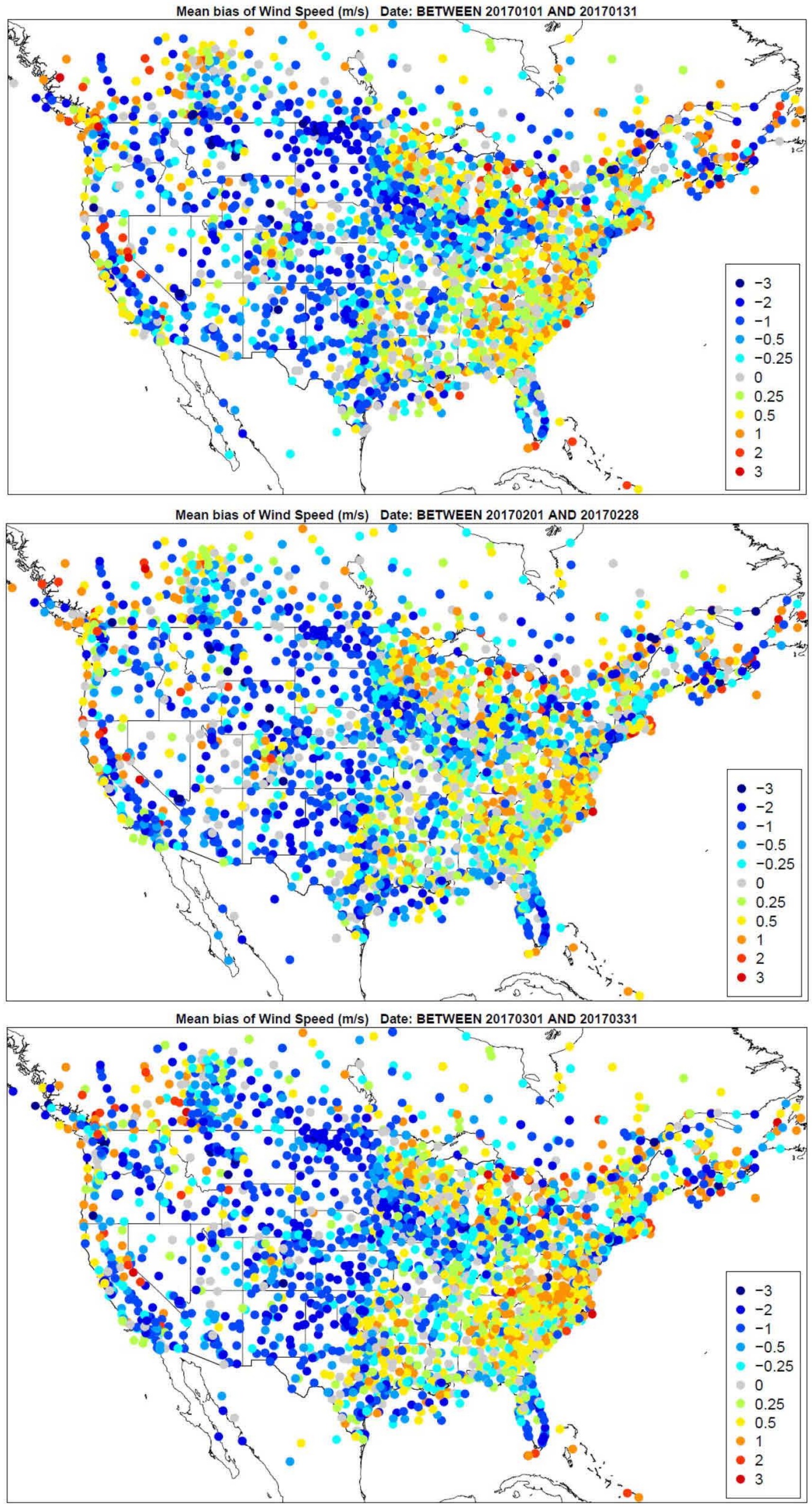

Figure 3.1.2. Spatial distribution of wind speed bias (m/s) across all hours for the months of January, February, and March (top to bottom).

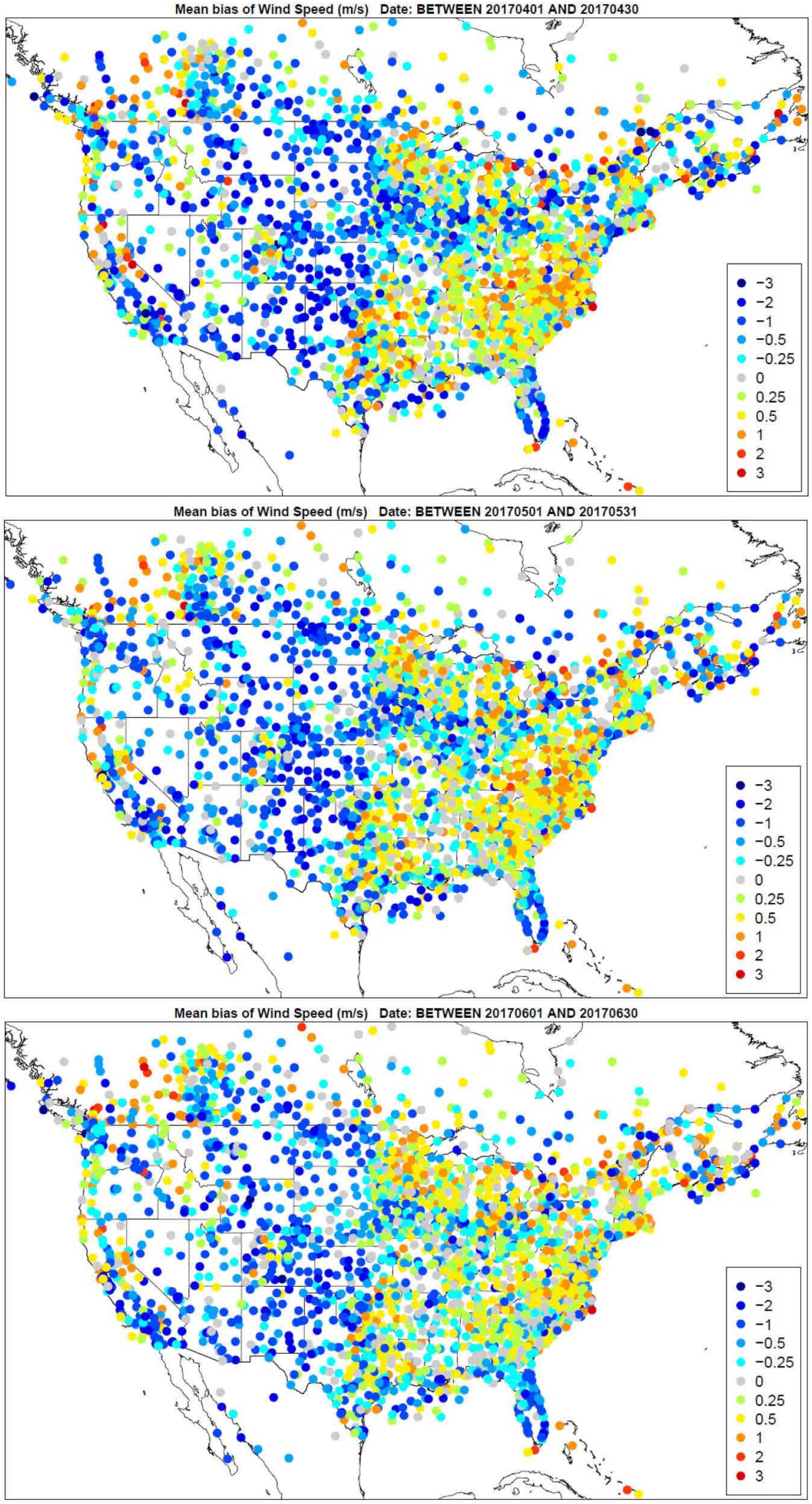

Figure 3.1.3. Spatial distribution of wind speed bias (m/s) across all hours for the months of April, May, and June (top to bottom).

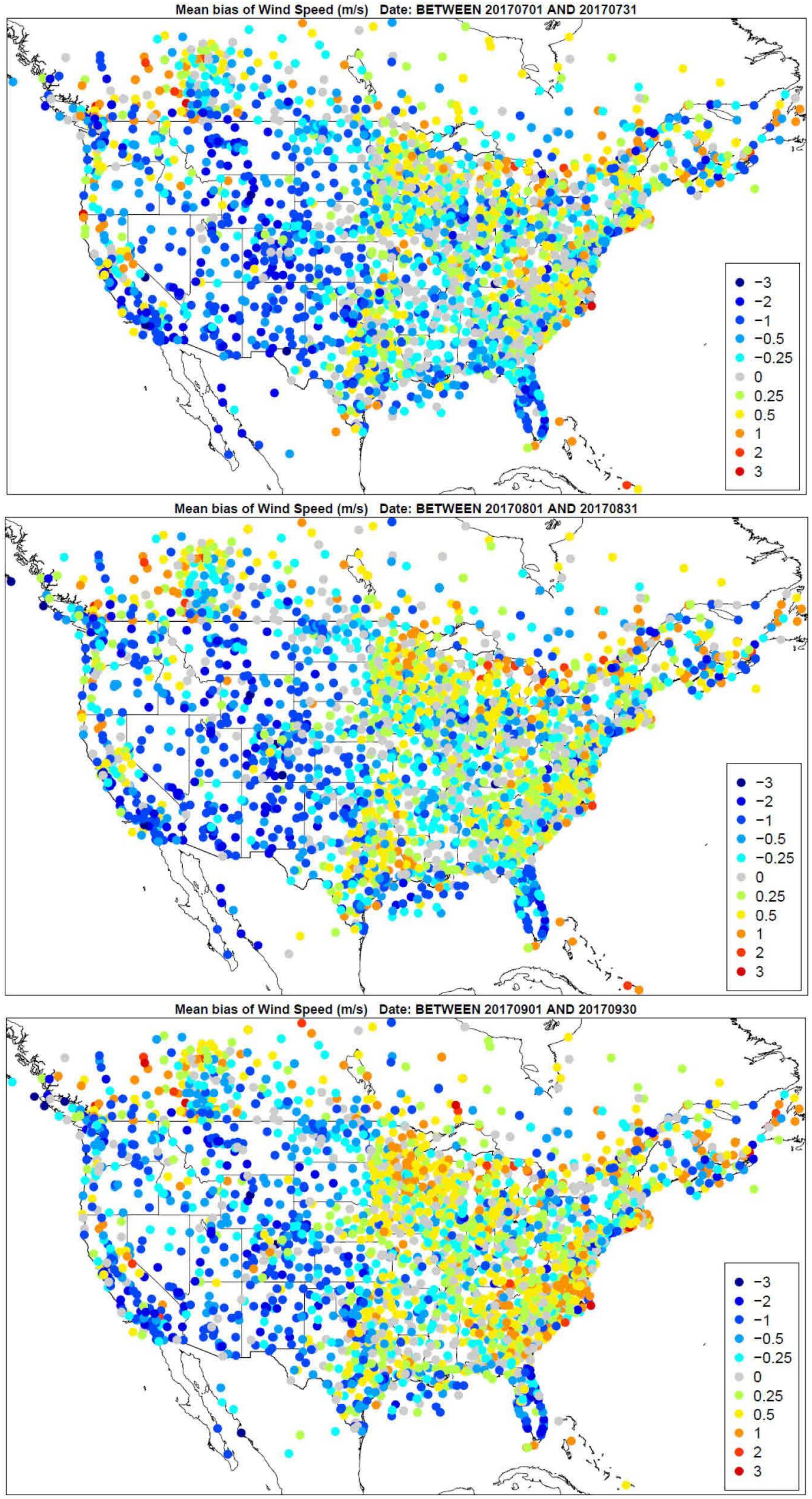

Figure 3.1.4. Spatial distribution of wind speed bias (m/s) across all hours for the months of July, August, and September (top to bottom).

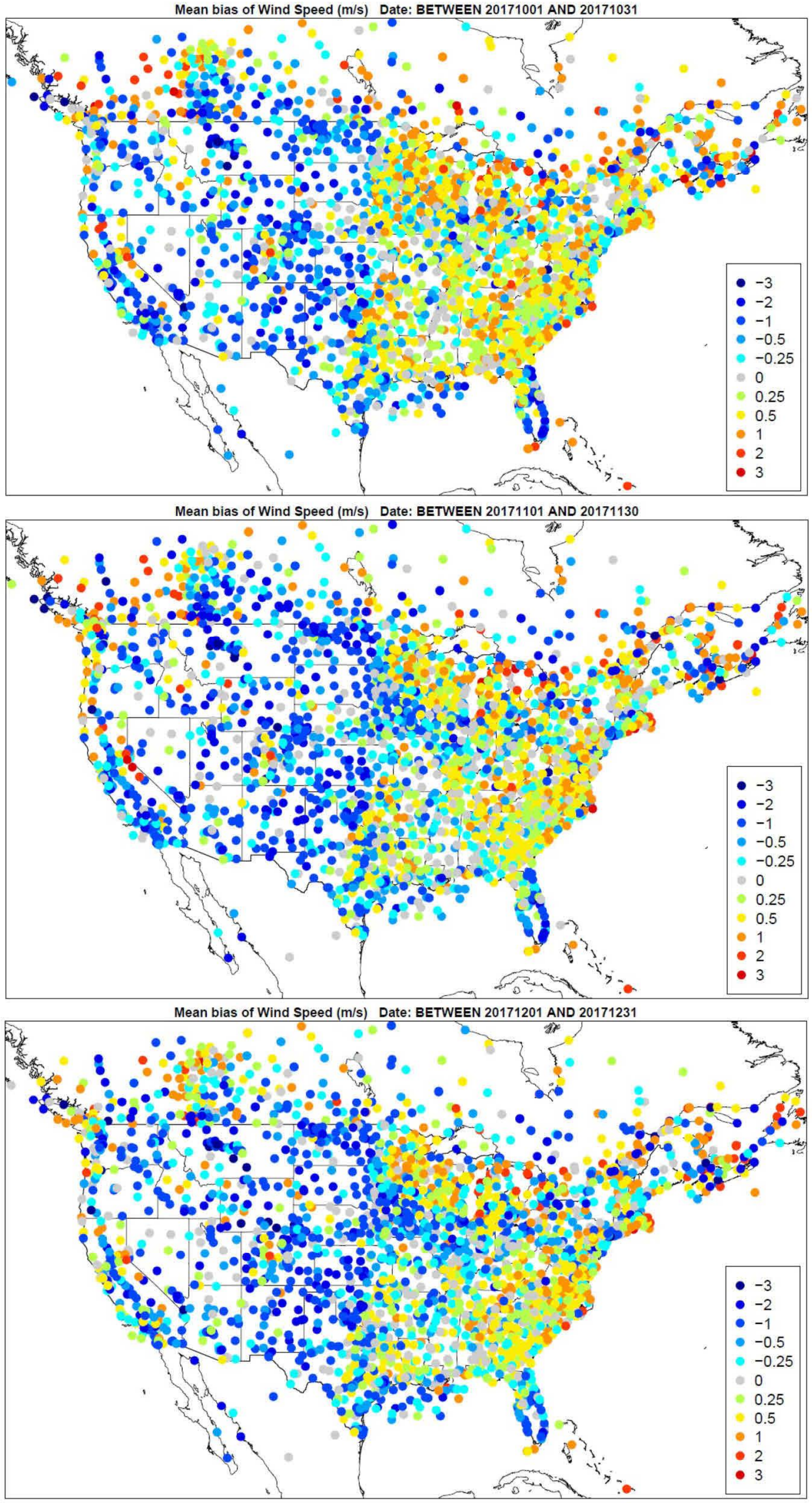

Figure 3.1.5. Spatial distribution of wind speed bias (m/s) across all hours for the months of October, November, and December (top to bottom).

Climate Region	Season	Mean Obs	Mean Mod	MB	MAE	NMB	NME	RMSE
Northeast	Q1	4.58	4.24	1.37	0.05	1.18	29.89	1.93
	Q2	4.04	3.75	1.22	0.05	1.24	30.11	1.72
	Q3	3.4	2.96	1.03	-0.02	-0.57	30.37	1.48
	Q4	4.08	3.71	1.26	0.12	2.89	30.81	1.82
N. Rockies & Plains	Q1	5.16	4.24	1.48	-0.69	-13.37	28.71	2
	Q2	5.04	4.26	1.39	-0.55	-10.91	27.48	1.86
	Q3	4.13	3.51	1.25	-0.38	-9.28	30.35	1.71
	Q4	5.27	4.47	1.43	-0.55	-10.48	27.19	1.95
Northwest	Q1	4.06	3.34	1.52	-0.39	-9.72	37.34	2.02
	Q2	3.96	3.35	1.33	-0.29	-7.45	33.59	1.75
	Q3	3.47	2.87	1.15	-0.32	-9.3	33.19	1.51
	Q4	3.77	3.08	1.38	-0.34	-9.02	36.6	1.83
Ohio Valley	Q1	4.55	4.17	1.11	-0.11	-2.48	24.44	1.46
	Q2	4.27	3.9	1.11	-0.01	-0.28	26.04	1.48
	Q3	3.14	2.7	0.89	-0.05	-1.47	28.19	1.18
	Q4	4.08	3.71	1.01	0.01	0.19	24.72	1.32
South	Q1	4.76	4.21	1.22	-0.3	-6.34	25.67	1.64
	Q2	4.72	4.18	1.25	-0.21	-4.38	26.39	1.68
	Q3	3.8	3.26	1.05	-0.17	-4.56	27.67	1.43
	Q4	4.27	3.69	1.08	-0.21	-4.82	25.3	1.45
Southeast	Q1	3.79	3.56	1.16	0.22	5.77	30.73	1.54
	Q2	3.64	3.34	1.14	0.17	4.72	31.42	1.52
	Q3	3.19	2.72	1.04	0.01	0.47	32.51	1.42
	Q4	3.41	3.09	1.05	0.21	6.19	30.85	1.4
Southwest	Q1	4.64	3.79	1.64	-0.57	-12.25	35.4	2.25
	Q2	4.74	3.88	1.62	-0.61	-12.84	34.19	2.19
	Q3	3.94	3.08	1.52	-0.67	-16.9	38.59	2.07
	Q4	4.34	3.47	1.57	-0.59	-13.68	36.22	2.2
Upper Midwest	Q1	4.61	4.3	1.15	-0.02	-0.46	24.85	1.52
	Q2	4.4	4.16	1.17	0.08	1.77	26.64	1.54
	Q3	3.48	3.36	1.02	0.27	7.69	29.18	1.34
	Q4	4.52	4.43	1.17	0.23	5.17	25.8	1.54
West	Q1	4.08	3.39	1.46	-0.31	-7.66	35.76	1.98
	Q2	4.32	3.61	1.36	-0.37	-8.54	31.47	1.82
	Q3	3.79	3.01	1.26	-0.5	-13.26	33.18	1.68
	Q4	3.54	2.81	1.31	-0.36	-10.14	36.89	1.77

Table 3.1.1. Mean observed, mean modeled, mean bias (MB), mean absolute error (MAE), normalized mean bias (NMB), normalized mean error (NME), and root mean square error (RMSE) for wind speed (m/s).

Wind vector displacement (km) is presented below (Figure 3.1.6) utilizing the ds472 observation network described earlier. These plots show the entire distribution of hourly wind displacement by month and by hour of the day. Overall, model performance is adequate in terms of wind vector differences. The average wind displacement for the WRF simulation is around 5km for all months and hours of the day. The interquartile ranges are roughly 2-10km. As the displacement is generally less than the resolution of the model, minimal impacts due to displacement of wind vectors are expected.

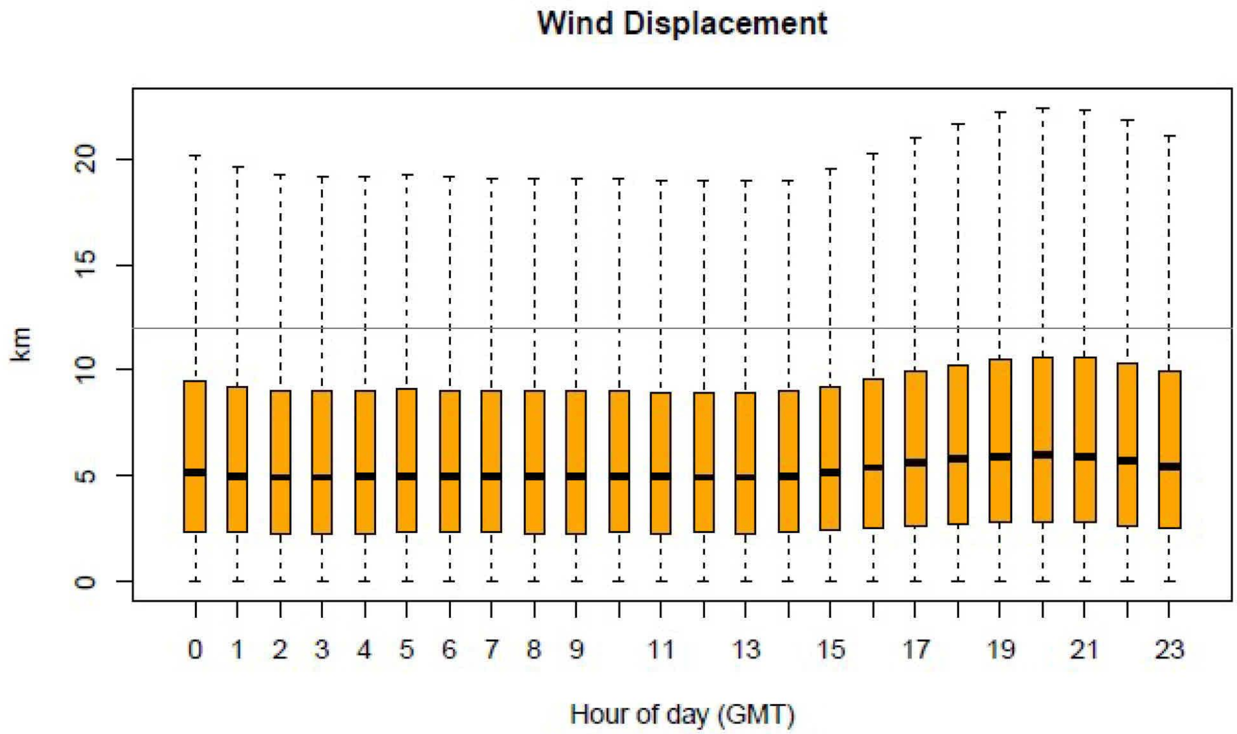

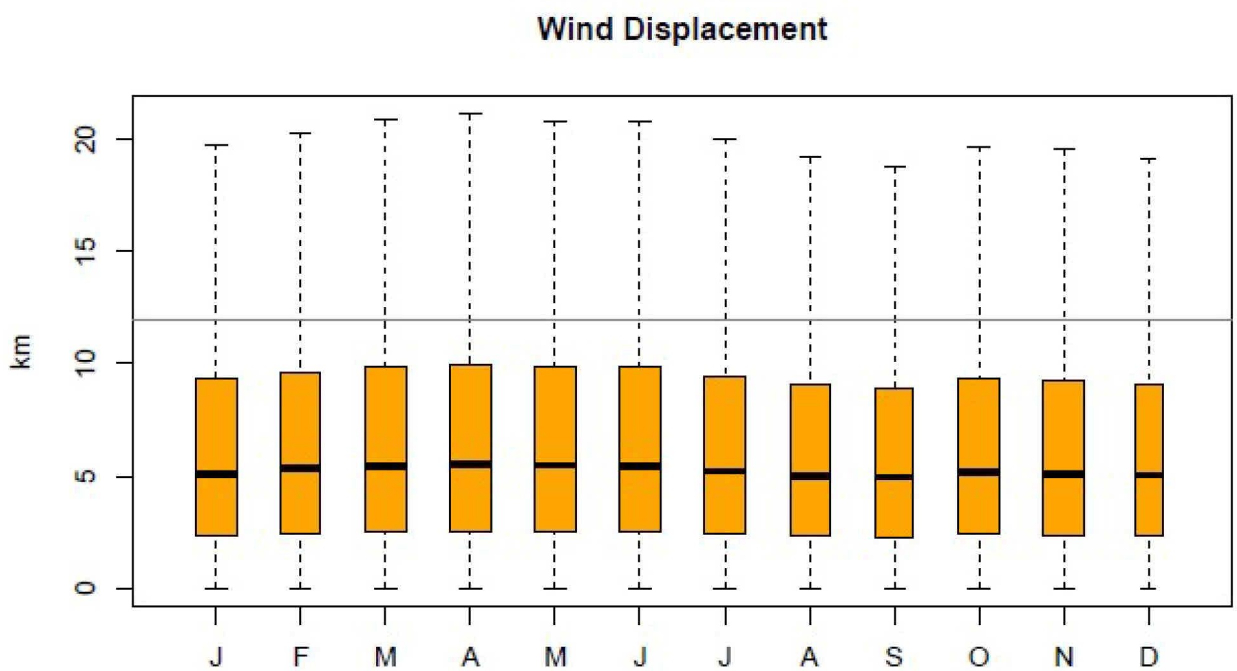

Figure 3.1.6. Distribution of hourly wind displacement by hour and month.

3.2 Temperature

Temperature estimates are compared to the ds472 observation network described earlier and are presented below (Figure 3.2.1). Regional analysis of statistical metrics for temperature performance by quarter is shown in Table 3.2.1.

Overall, WRF slightly overpredicts temperatures across most months of the year. The range of biases decreases slightly during the late spring and early summer months (April-July) compared to the rest of the year, with the inner-quartile range (IQR) becoming more tightly centered around zero. Model error decreases considerably during the late spring and much of the summer, as well. Overall, with an average IQR of +/- 1 degree, this is considered adequate model performance.

In Figures 3.2.3-3.2.6, spatial distribution of monthly biases is presented across all hours. WRF generally overpredicts temperatures slightly across most months of the year. A more noticeable overprediction is noted during the months of July, October, and December, with an overprediction on the order of 1 to 1.5 degrees. In areas of the western US, performance for temperature is mixed, with persistent significant overpredictions and underpredictions observed in varying locations.

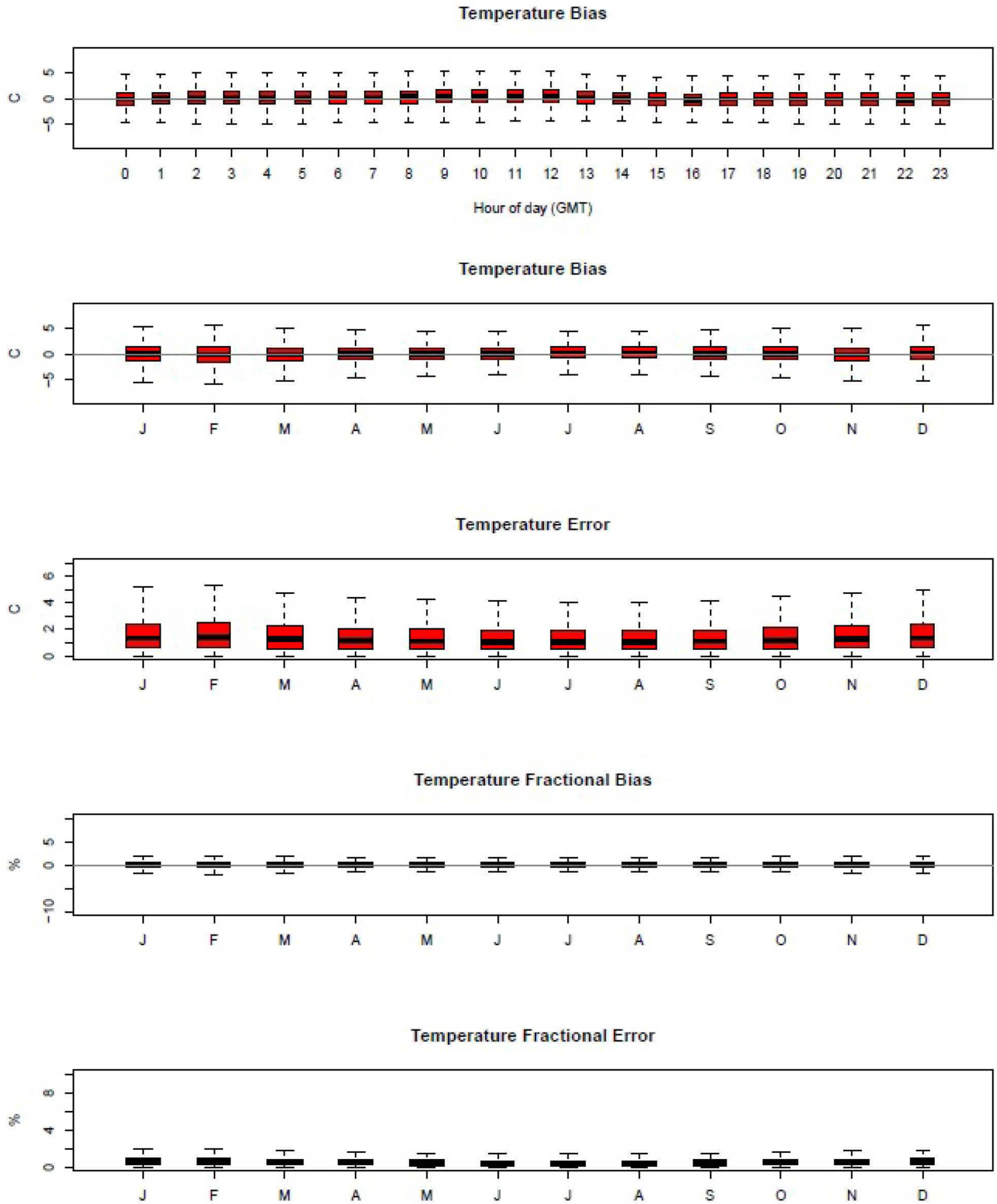

Figure 3.2.1. Distribution of hourly bias by hour and hourly bias, error, fractional bias, and fractional error for temperature by month.

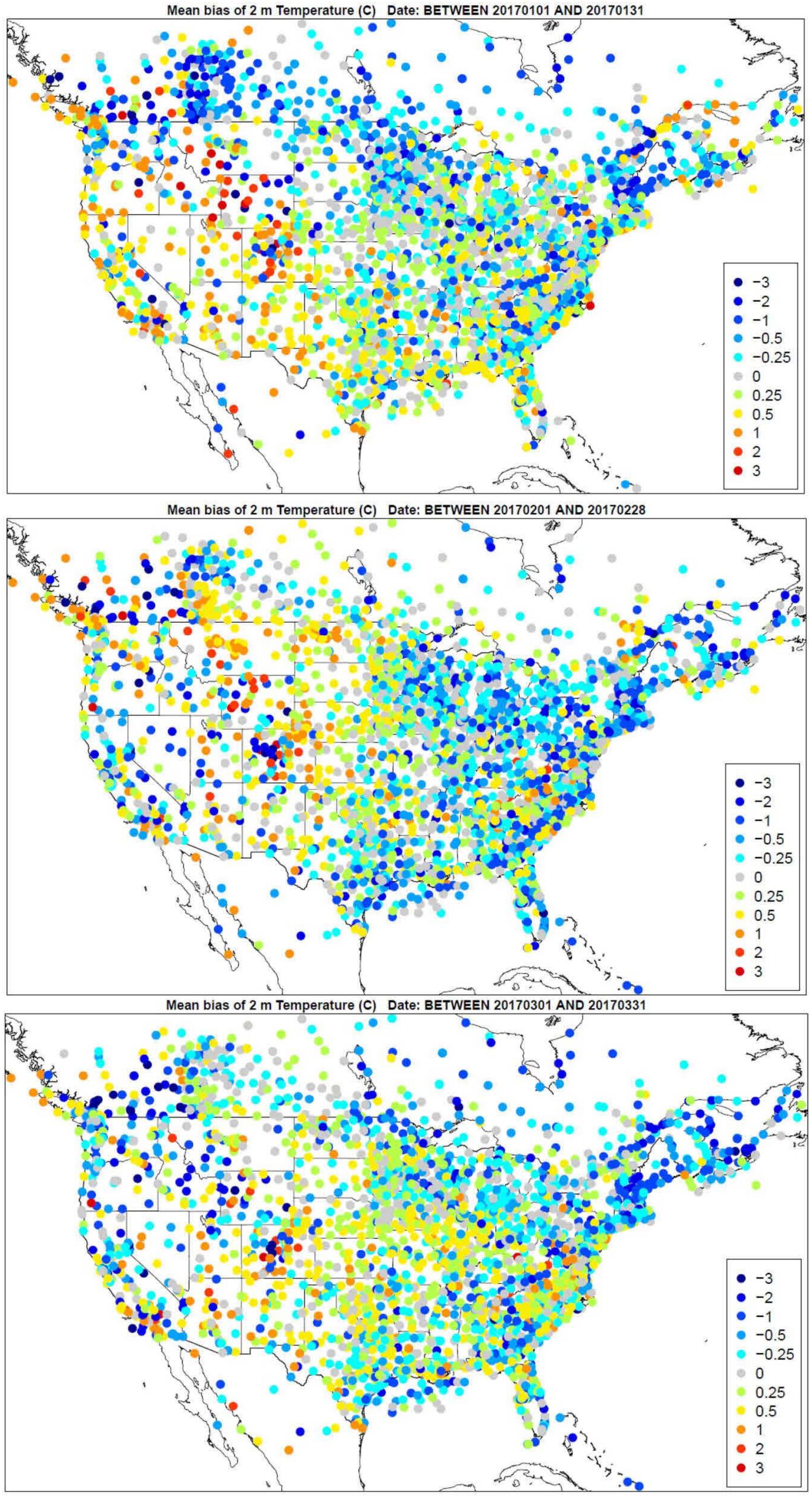

Figure 3.2.2. Spatial distribution of temperature bias (C) across all hours for the months of January, February, and March (top to bottom).

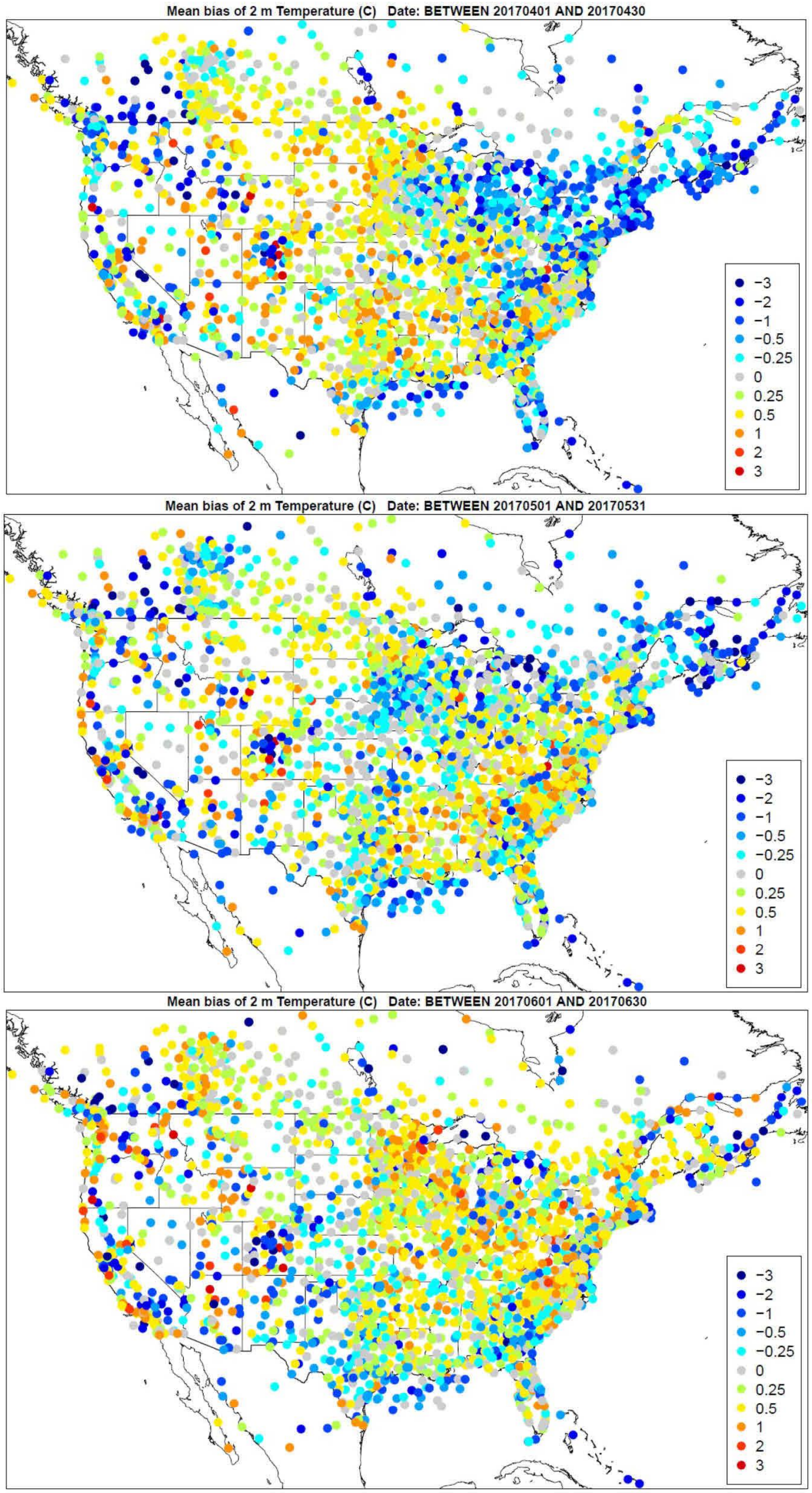

Figure 3.2.3. Spatial distribution of temperature bias (C) across all hours for the months of April, May, and June (top to bottom).

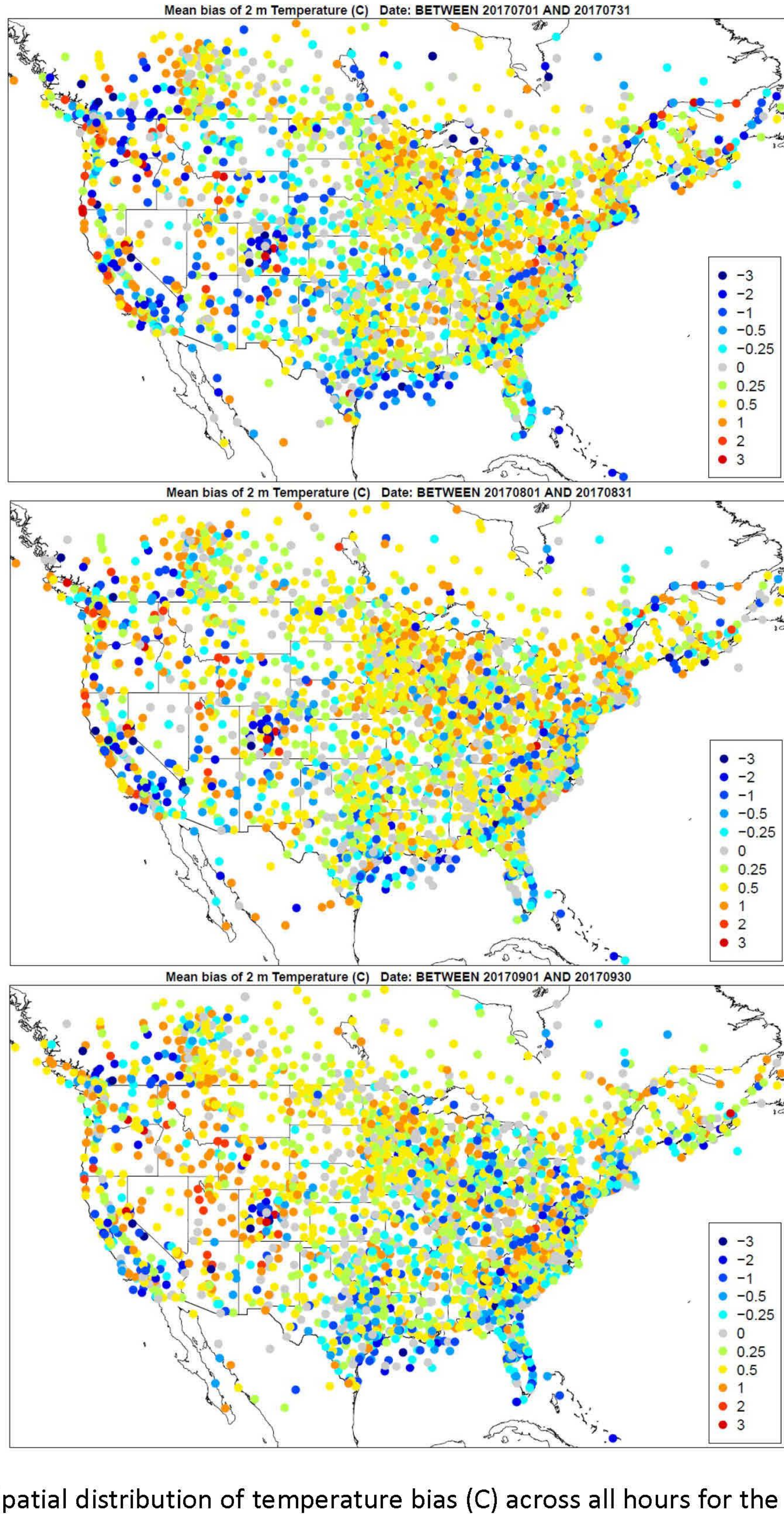

Figure 3.2.4. Spatial distribution of temperature bias (C) across all hours for the months of July, August, and September (top to bottom).

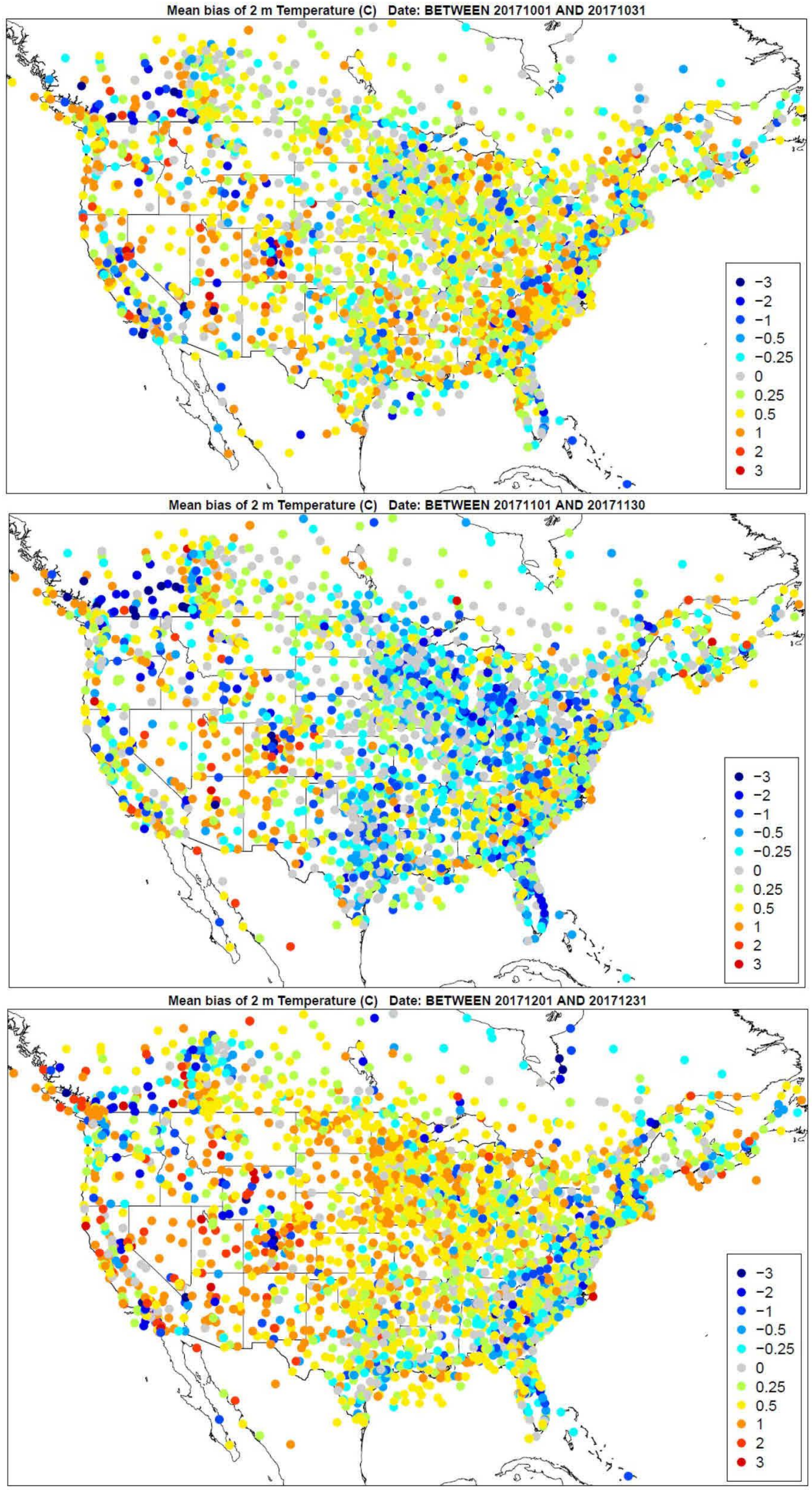

Figure 3.2.5. Spatial distribution of temperature bias (C) across all hours for the months of October, November, and December (top to bottom).

Climate Region	Season	Mean Obs	Mean Mod	MB	MAE	NMB	NME	RMSE
Northeast	Q1	274.49	1.17	1.77	-0.18	-0.06	0.64	2.35
	Q2	288.27	288.34	1.5	0.07	0.02	0.52	2.03
	Q3	293.59	294.02	1.33	0.43	0.15	0.45	1.79
	Q4	279.4	279.65	1.67	0.25	0.09	0.6	2.21
N. Rockies & Plains	Q1	271.24	271.54	2.07	0.31	0.11	0.76	2.78
	Q2	286.57	286.86	1.54	0.29	0.1	0.54	2.02
	Q3	293	293.36	1.67	0.36	0.12	0.57	2.19
	Q4	275.13	275.56	1.98	0.42	0.15	0.72	2.58
Northwest	Q1	275.27	275.45	1.83	0.17	0.06	0.66	2.51
	Q2	286.22	286.42	1.51	0.19	0.07	0.53	2
	Q3	292.78	293.35	1.87	0.57	0.2	0.64	2.48
	Q4	278.28	278.72	1.79	0.45	0.16	0.64	2.38
Ohio Valley	Q1	278.25	278.29	1.59	0.03	0.01	0.57	2.06
	Q2	291.21	291.54	1.35	0.33	0.11	0.46	1.77
	Q3	295.12	295.55	1.25	0.43	0.15	0.42	1.65
	Q4	280.53	280.84	1.61	0.3	0.11	0.57	2.06
South	Q1	286.41	286.58	1.75	0.17	0.06	0.61	2.25
	Q2	295.37	295.62	1.28	0.24	0.08	0.43	1.72
	Q3	299.39	299.63	1.22	0.24	0.08	0.41	1.62
	Q4	287.16	287.48	1.71	0.32	0.11	0.59	2.2
Southeast	Q1	285.95	286	1.73	0.04	0.02	0.6	2.25
	Q2	295.09	295.32	1.33	0.23	0.08	0.45	1.76
	Q3	298.32	298.54	1.21	0.21	0.07	0.41	1.6
	Q4	287.25	287.48	1.61	0.23	0.08	0.56	2.09
Southwest	Q1	278.36	278.69	2.1	0.34	0.12	0.75	2.79
	Q2	289.61	289.85	1.91	0.24	0.08	0.66	2.54
	Q3	294.72	295.04	1.98	0.32	0.11	0.67	2.64
	Q4	280.85	281.55	2.32	0.7	0.25	0.83	3
Upper Midwest	Q1	270.63	270.57	1.46	-0.06	-0.02	0.54	1.92
	Q2	286.82	287	1.47	0.17	0.06	0.51	1.94
	Q3	292.36	292.83	1.32	0.47	0.16	0.45	1.74
	Q4	274.83	275.11	1.51	0.28	0.1	0.55	1.98
West	Q1	283.84	283.97	1.61	0.13	0.05	0.57	2.18
	Q2	291.64	291.75	1.68	0.11	0.04	0.57	2.24
	Q3	296.71	296.89	1.81	0.18	0.06	0.61	2.45
	Q4	286.54	287.07	2.1	0.53	0.18	0.73	2.8

Table 3.2.1. Mean observed, mean modeled, mean bias (MB), mean absolute error (MAE), normalized mean bias (NMB), normalized mean error (NME), and root mean square error (RMSE) for temperature (K).

3.3 Mixing Ratio

Water mixing ratio estimates are compared to the ds472 observation network described earlier and are presented below (Figure 3.3.1). Regional analysis of statistical metrics for water vapor mixing ratio performance by quarter is shown in Table 3.3.1.

The WRF simulation slightly overpredicts moisture across most hours of the day, with a more noticeable overprediction during the late evening and overnight hours. Additionally, there is more uncertainty in model predictions during the spring and summer months. This increase in error is explained by the increased convective activity and influx of moist air masses that are typical of that time of year. In general, WRF performance was adequate for water vapor mixing ratio.

The monthly spatial distributions of the mixing ratio bias across all hours are shown in Figures 3.3.3-3.3.6. As noted in the earlier figures, a general overprediction of moisture is observed across much of the year. Some slight variations appear across regions, with a noticeable underprediction of moisture that persists across the Southeast for much of the year. Mixing ratio performance is noticeably overpredicted during the summer months across the Western US, with biases of 1-2 g/kg.

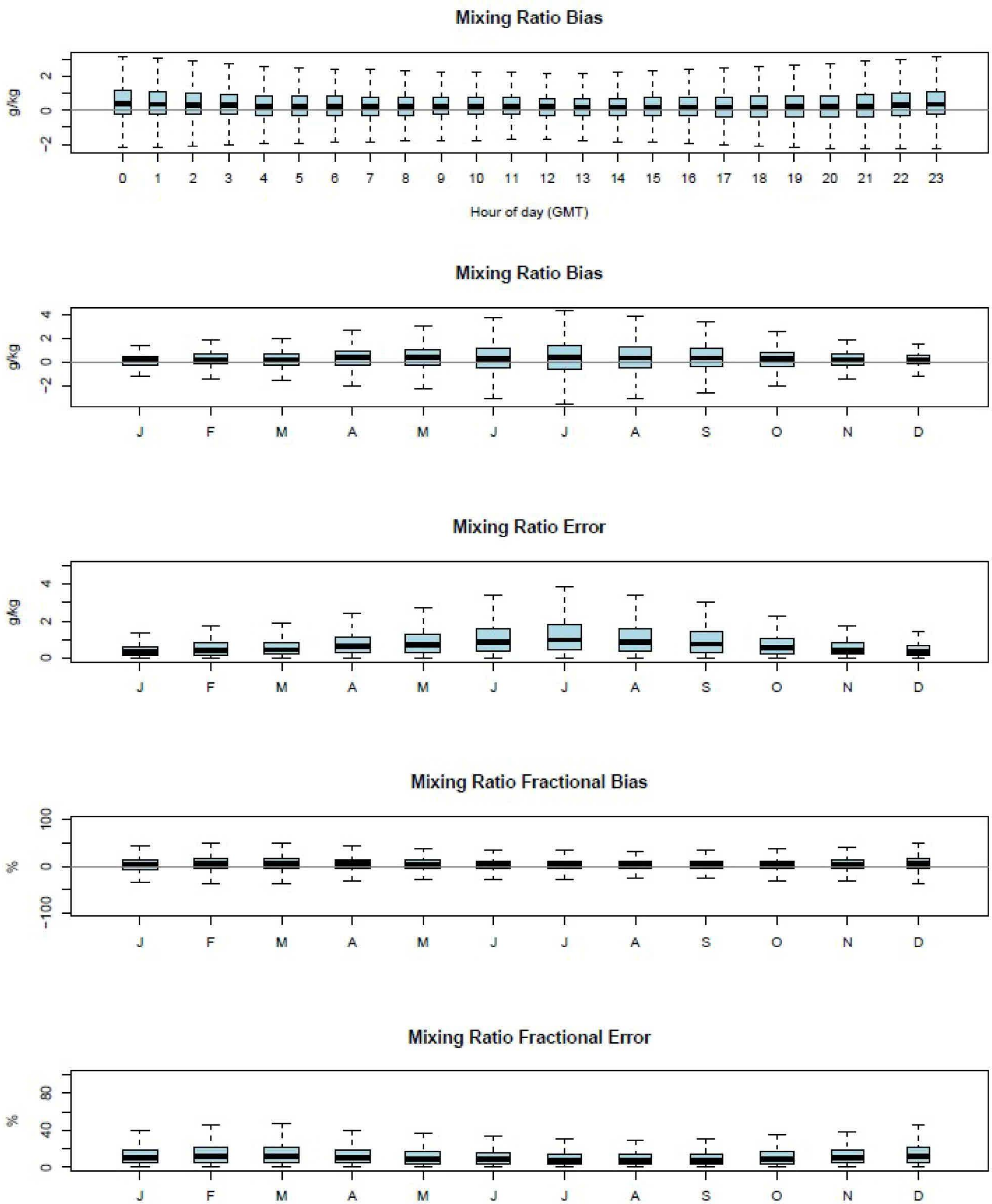

Figure 3.3.1. Distribution of hourly bias by hour and hourly bias, error, fractional bias, and fractional error for water vapor mixing ratio by month.

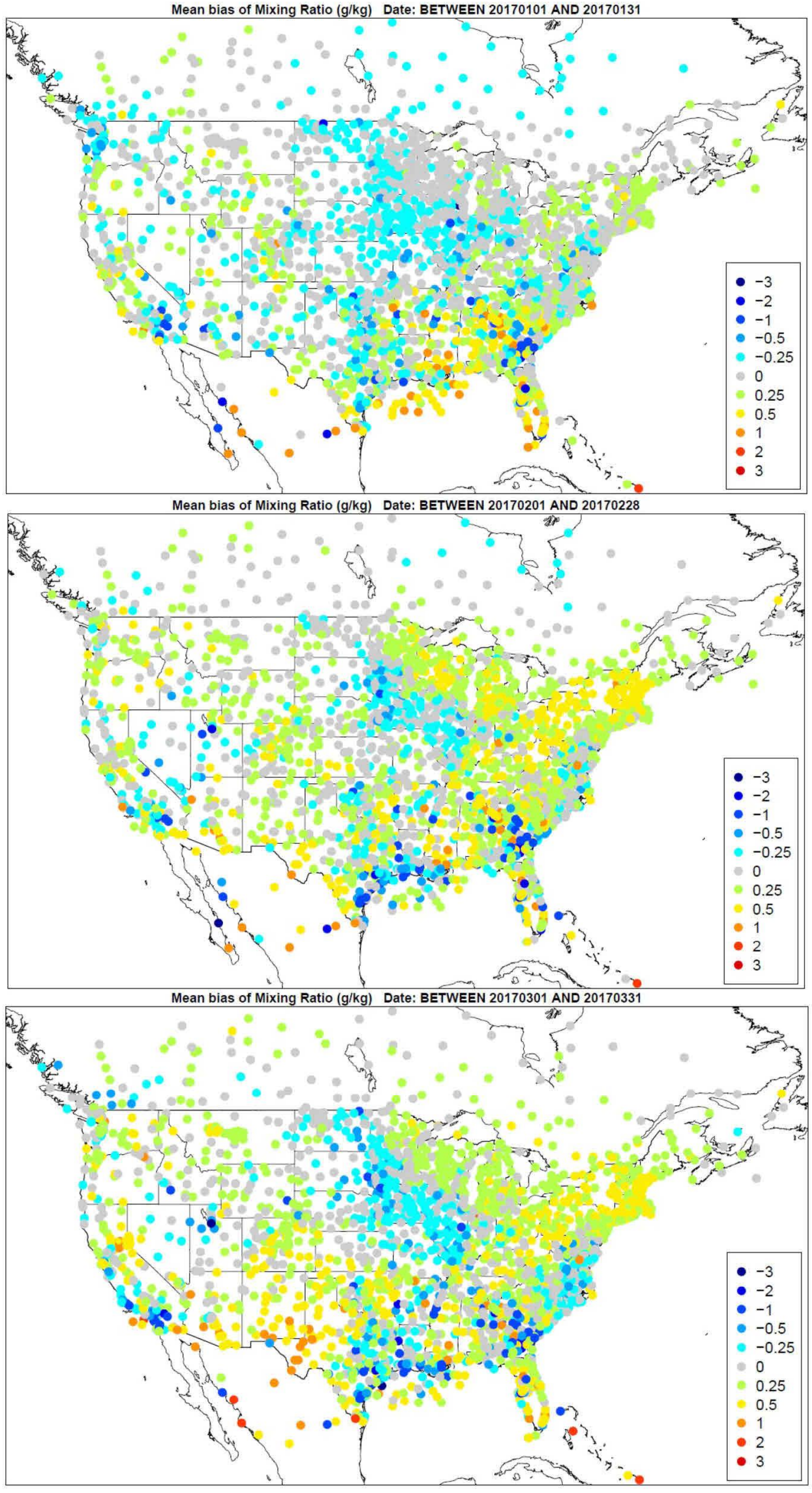

Figure 3.3.2. Spatial distribution of water vapor mixing ratio bias (g/kg) across all hours for the months of January, February, and March (top to bottom).

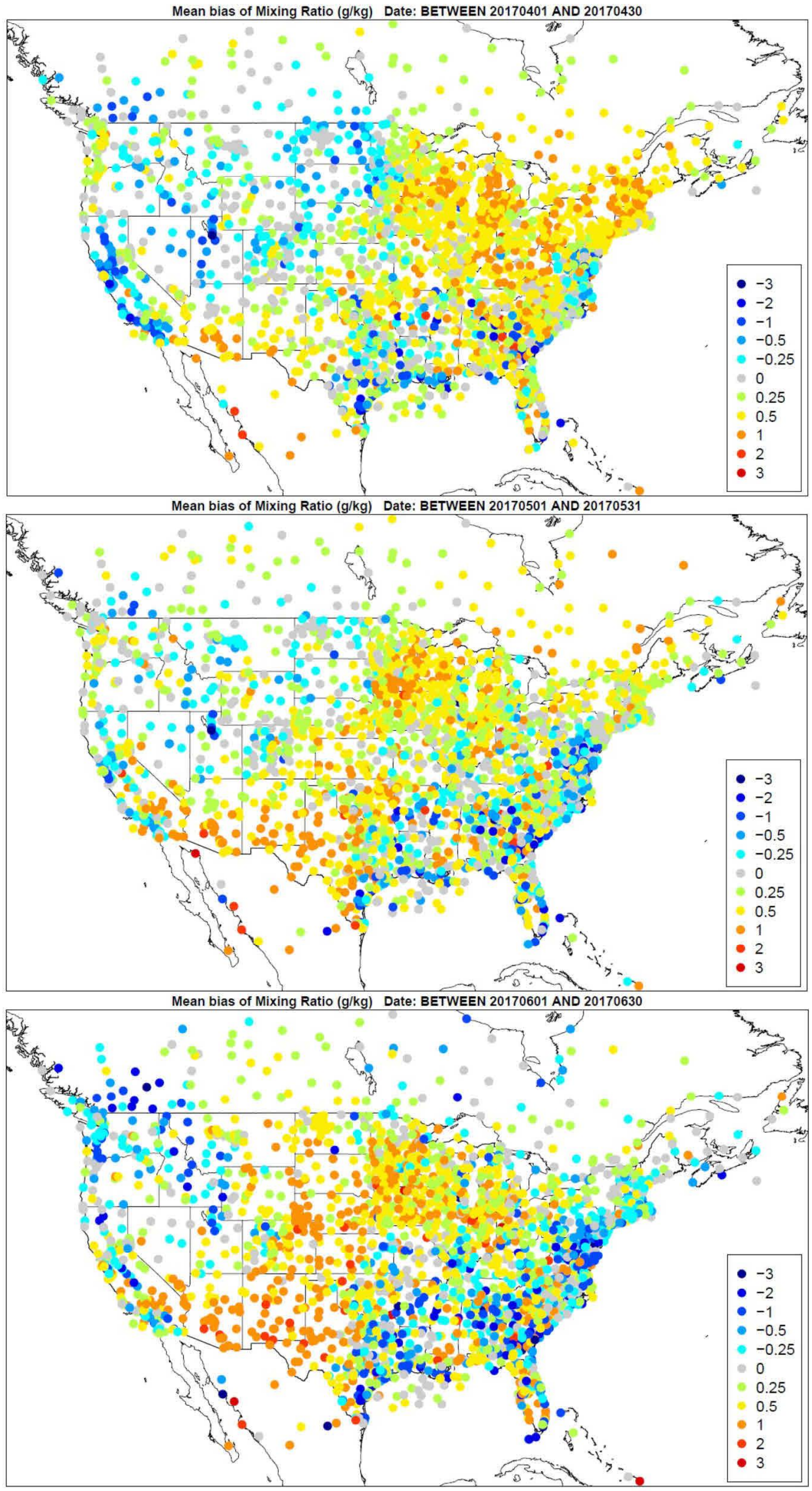

Figure 3.3.3. Spatial distribution of water vapor mixing ratio bias (g/kg) across all hours for the months of April, May, and June (top to bottom).

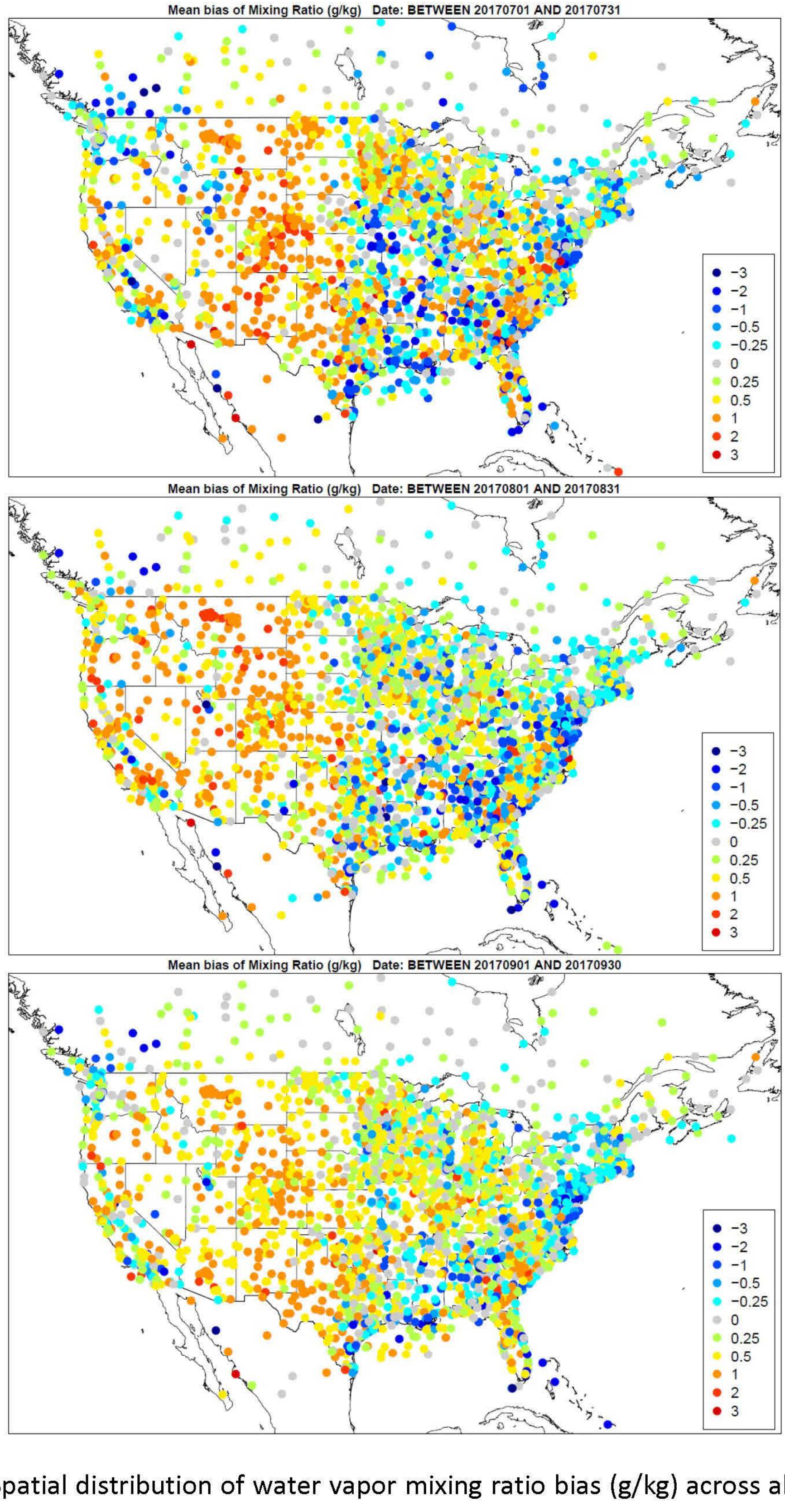

Figure 3.3.4. Spatial distribution of water vapor mixing ratio bias (g/kg) across all hours for the months of July, August, and September (top to bottom).

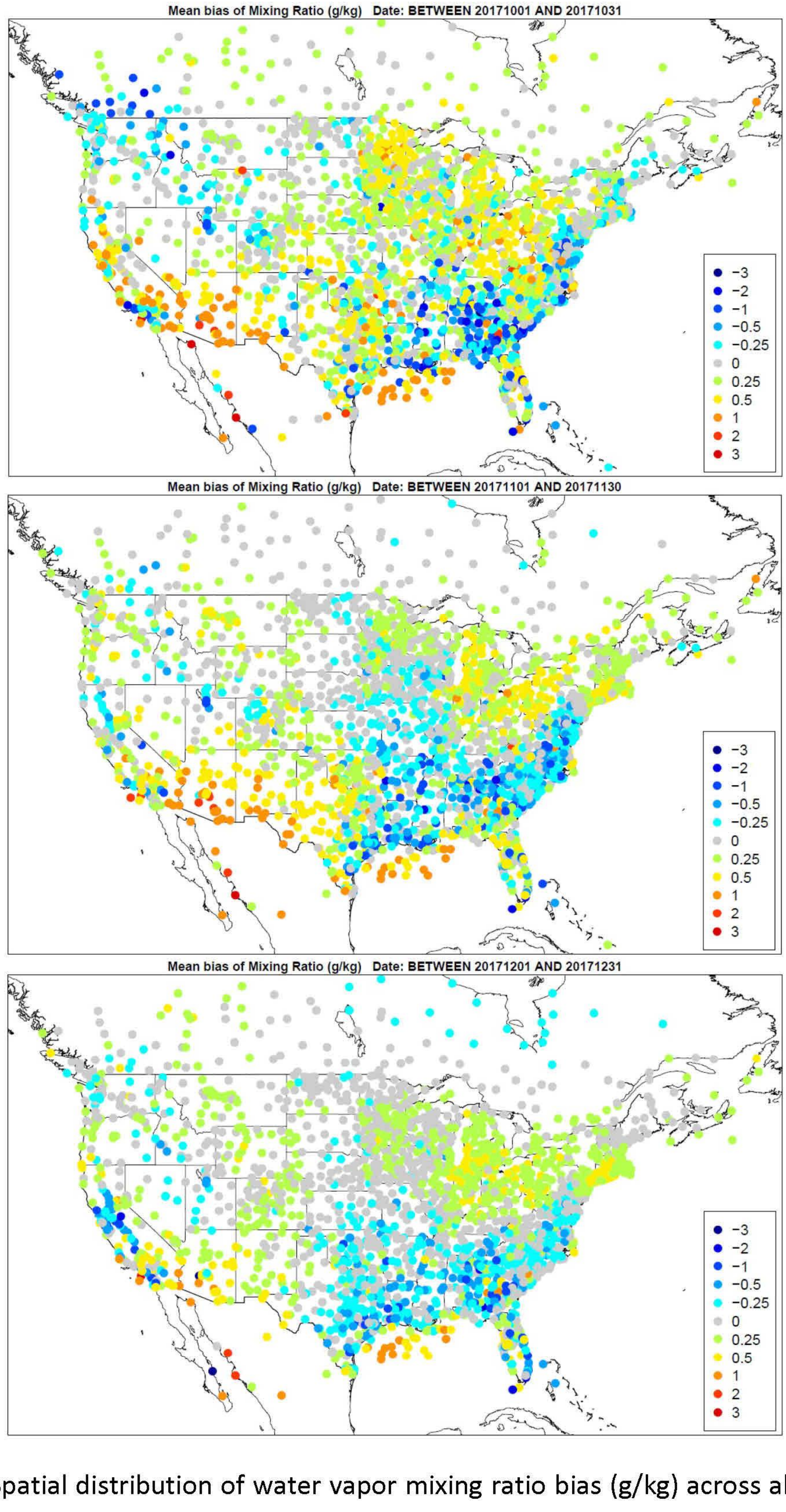

Figure 3.3.5. Spatial distribution of water vapor mixing ratio bias (g/kg) across all hours for the months of October, November, and December (top to bottom).

Climate Region	Season	Mean Obs	Mean Mod	MB	MAE	NMB	NME	RMSE
Northeast	Q1	3.23	3.61	0.53	0.38	11.83	16.44	0.74
	Q2	8.02	8.39	0.88	0.37	4.63	10.97	1.19
	Q3	11.83	11.87	0.92	0.05	0.39	7.75	1.22
	Q4	5.2	5.47	0.56	0.27	5.14	10.82	0.76
N. Rockies & Plains	Q1	2.84	2.99	0.43	0.15	5.17	15.15	0.6
	Q2	6.28	6.63	0.87	0.35	5.61	13.89	1.21
	Q3	9.24	10.06	1.31	0.83	8.95	14.14	1.72
	Q4	3.37	3.56	0.44	0.19	5.69	13.19	0.61
Northwest	Q1	3.98	4.19	0.5	0.22	5.46	12.6	0.67
	Q2	6.21	6.35	0.71	0.14	2.32	11.45	0.98
	Q3	7.6	8.12	1.08	0.52	6.82	14.21	1.48
	Q4	4.63	4.76	0.54	0.13	2.89	11.7	0.72
Ohio Valley	Q1	4.45	4.64	0.55	0.19	4.28	12.34	0.78
	Q2	9.31	9.82	1.01	0.51	5.45	10.82	1.36
	Q3	12.87	13.19	1.04	0.31	2.43	8.11	1.4
	Q4	5.39	5.68	0.6	0.28	5.26	11.13	0.82
South	Q1	7.2	7.4	0.79	0.21	2.88	11.04	1.12
	Q2	12.23	12.61	1.11	0.38	3.09	9.04	1.51
	Q3	15.44	15.85	1.28	0.4	2.62	8.29	1.69
	Q4	7.81	8	0.8	0.18	2.34	10.24	1.1
Southeast	Q1	6.86	7.12	0.83	0.26	3.73	12.04	1.12
	Q2	12.42	12.67	1.13	0.25	2	9.11	1.51
	Q3	16.06	16.31	1.27	0.26	1.59	7.89	1.67
	Q4	8.61	8.61	0.8	0	0.02	9.28	1.09
Southwest	Q1	3.45	3.75	0.61	0.3	8.8	17.78	0.82
	Q2	4.72	5.28	1.03	0.57	12.05	21.77	1.38
	Q3	8.64	9.62	1.5	0.98	11.37	17.38	1.92
	Q4	3.49	3.9	0.73	0.41	11.88	20.97	1.03
Upper Midwest	Q1	2.85	2.98	0.38	0.14	4.79	13.35	0.54
	Q2	7.03	7.64	0.96	0.6	8.55	13.61	1.3
	Q3	10.98	11.36	0.97	0.38	3.45	8.81	1.3
	Q4	3.9	4.18	0.47	0.28	7.17	11.96	0.66
West	Q1	5.84	6	0.7	0.16	2.77	12.03	1
	Q2	6.92	7.08	0.93	0.16	2.27	13.37	1.29
	Q3	9.13	9.67	1.22	0.54	5.87	13.41	1.68
	Q4	5.24	5.52	0.95	0.28	5.42	18.24	1.37

Table 3.3.1. Mean observed, mean modeled, mean bias (MB), mean absolute error (MAE), normalized mean bias (NMB), normalized mean error (NME), and root mean square error (RMSE) for water vapor mixing ratio (g/kg).

3.4 Precipitation

Monthly total rainfall is plotted for each grid cell to assess how well the model captures the spatial variability and magnitude of convective and non-convective rainfall. As described earlier, the PRISM estimations for rainfall are only within the continental United States. WRF rainfall estimates by month are shown for all grid cells in the domain. Monthly total estimates are shown in Figures 3.4.1 through 3.4.12.

In general, WRF performs adequately in terms of the spatial patterns and magnitude of precipitation across the US throughout the year. WRF struggles with representing precipitation in areas of complex terrain (e.g., northern CA), particularly during the late winter and early spring months. In general, the simulation overpredicts precipitation across the western areas of the country during most months, with notable overpredictions of precipitation during periods of enhanced convective activity. Significant overpredictions are noted in the south-central US during May and across the desert Southwest and Front Range of the Rockies during July and August. The Deep South has a noted underprediction that persist across much of the year.

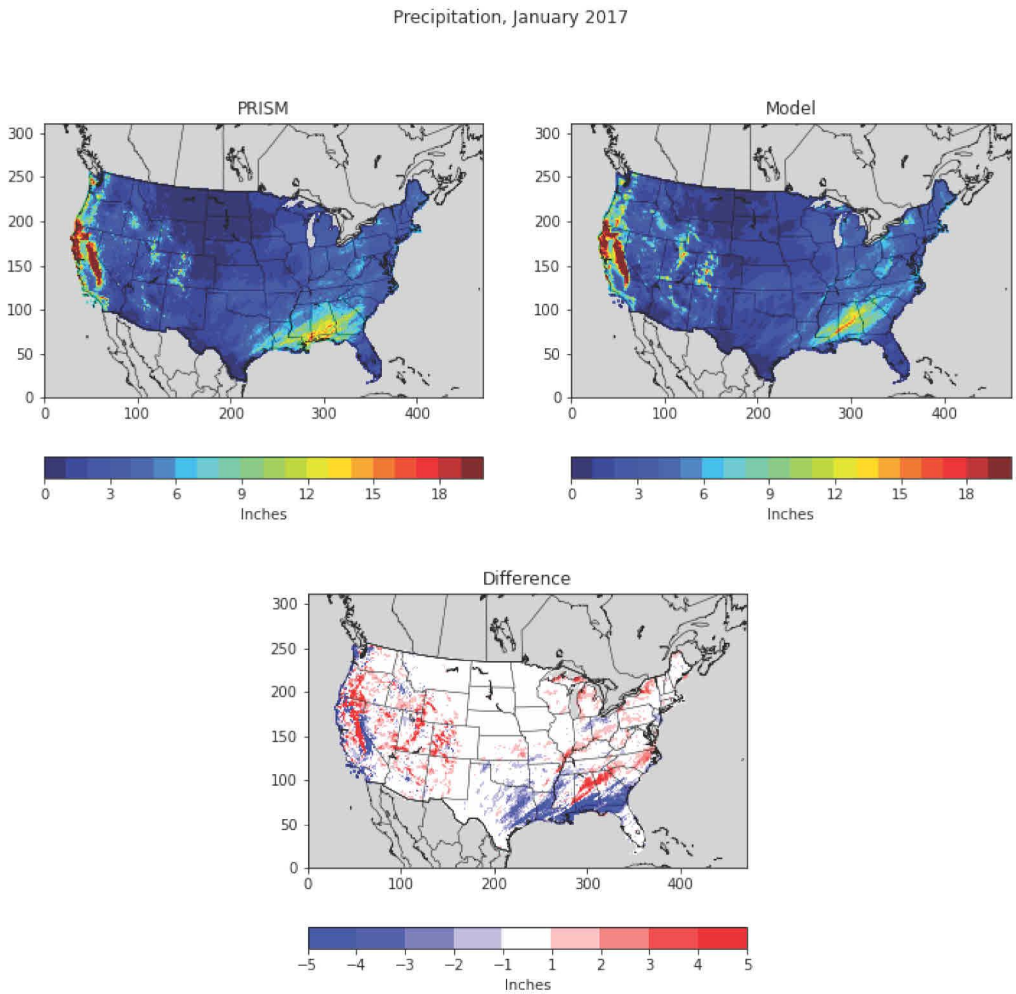

Figure 3.4.1. PRISM analysis (top left) and WRF (top right) estimated monthly total rainfall (in) and the difference (bottom) for January.

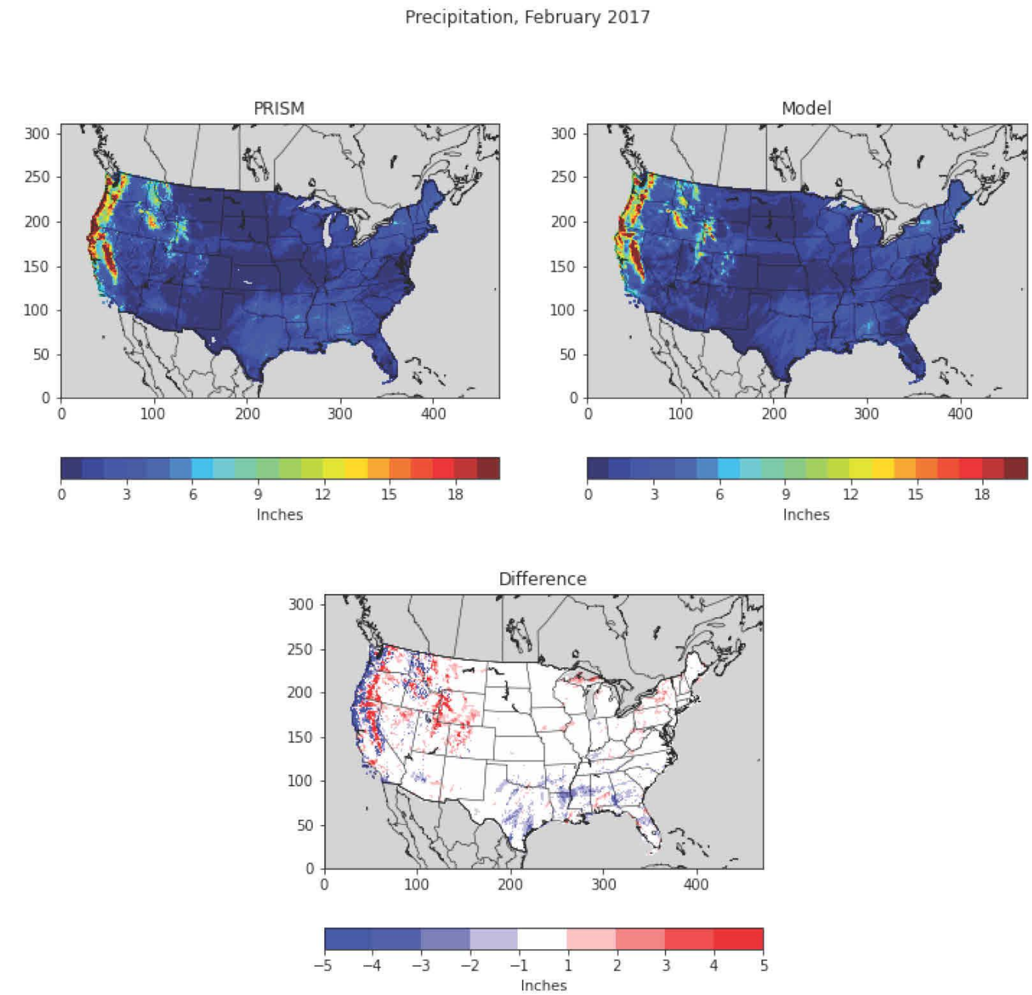

3.4.2. PRISM analysis (top left) and WRF (top right) estimated monthly total rainfall (in) and the difference (bottom) for February.

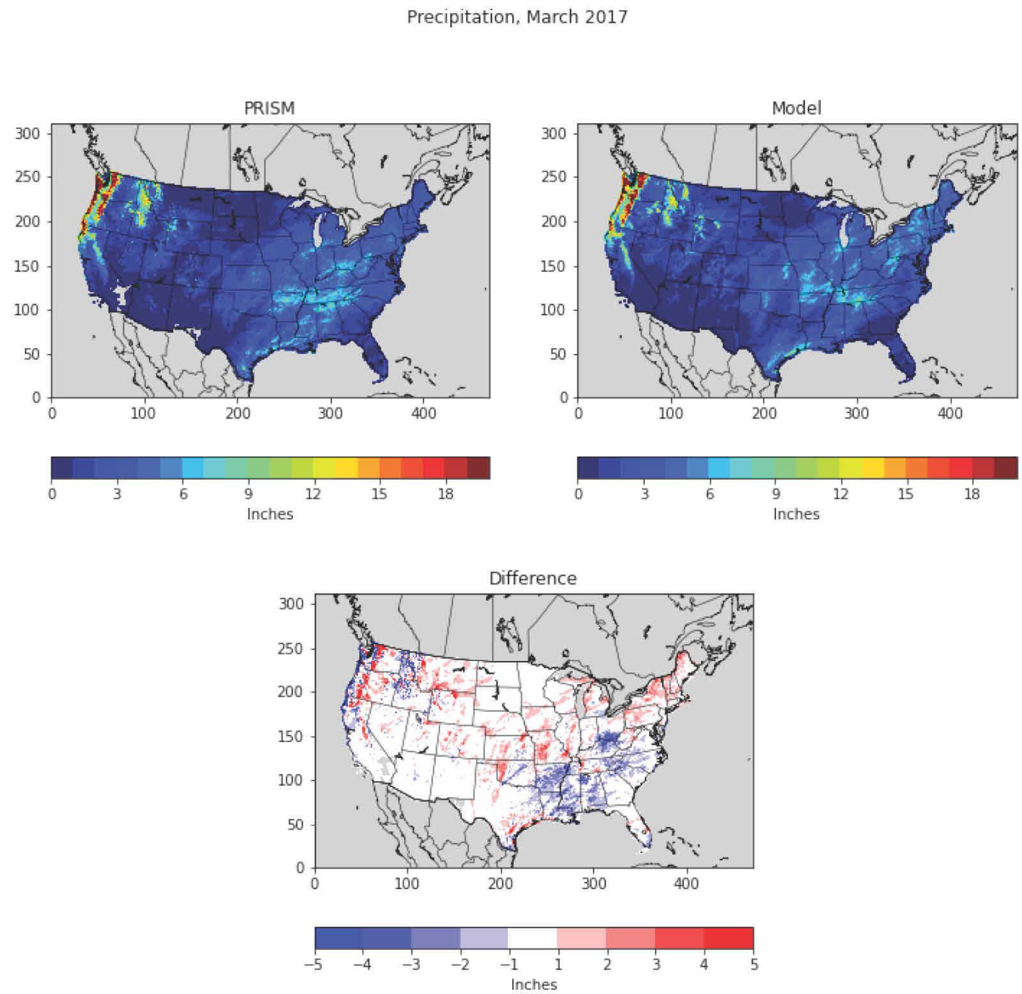

Figure 3.4.3. PRISM analysis (top left) and WRF (top right) estimated monthly total rainfall (in) and the difference (bottom) for March.

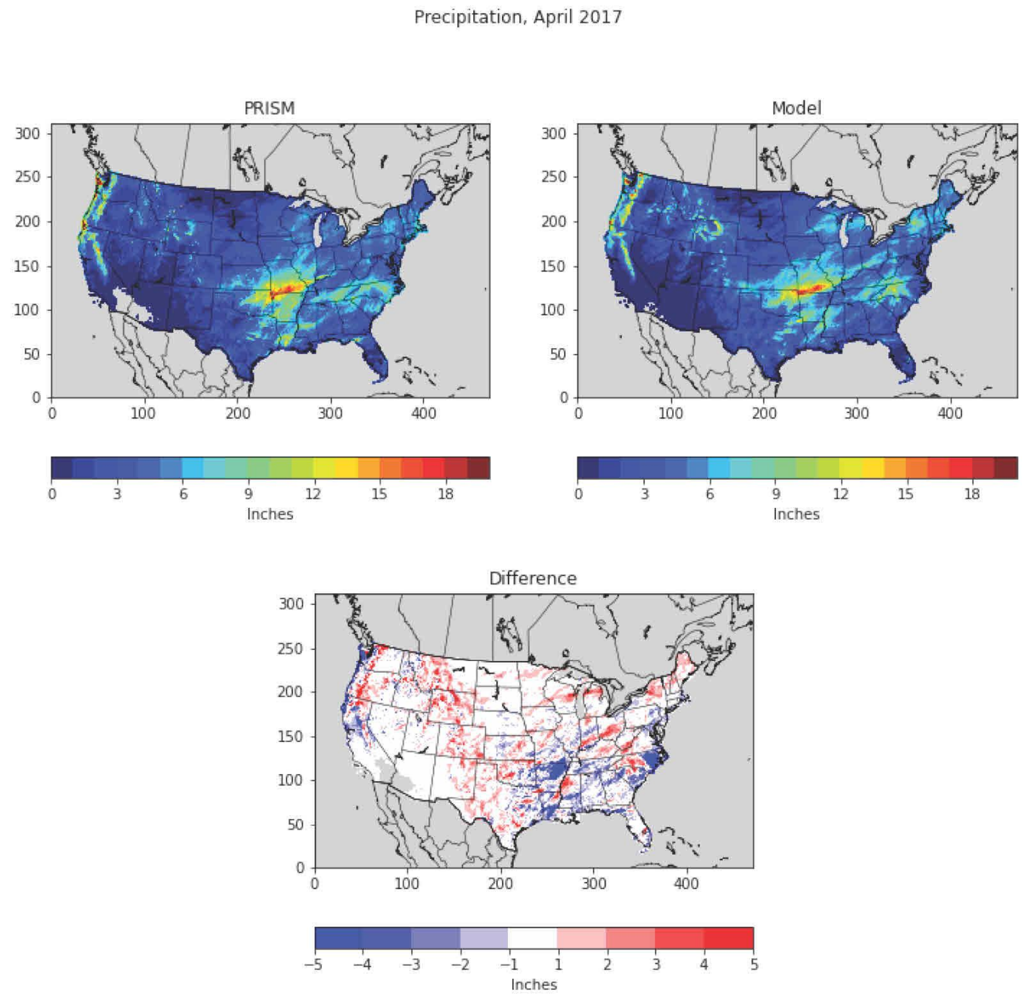

Figure 3.4.4. PRISM analysis (top left) and WRF (top right) estimated monthly total rainfall (in) and the difference (bottom) for April.

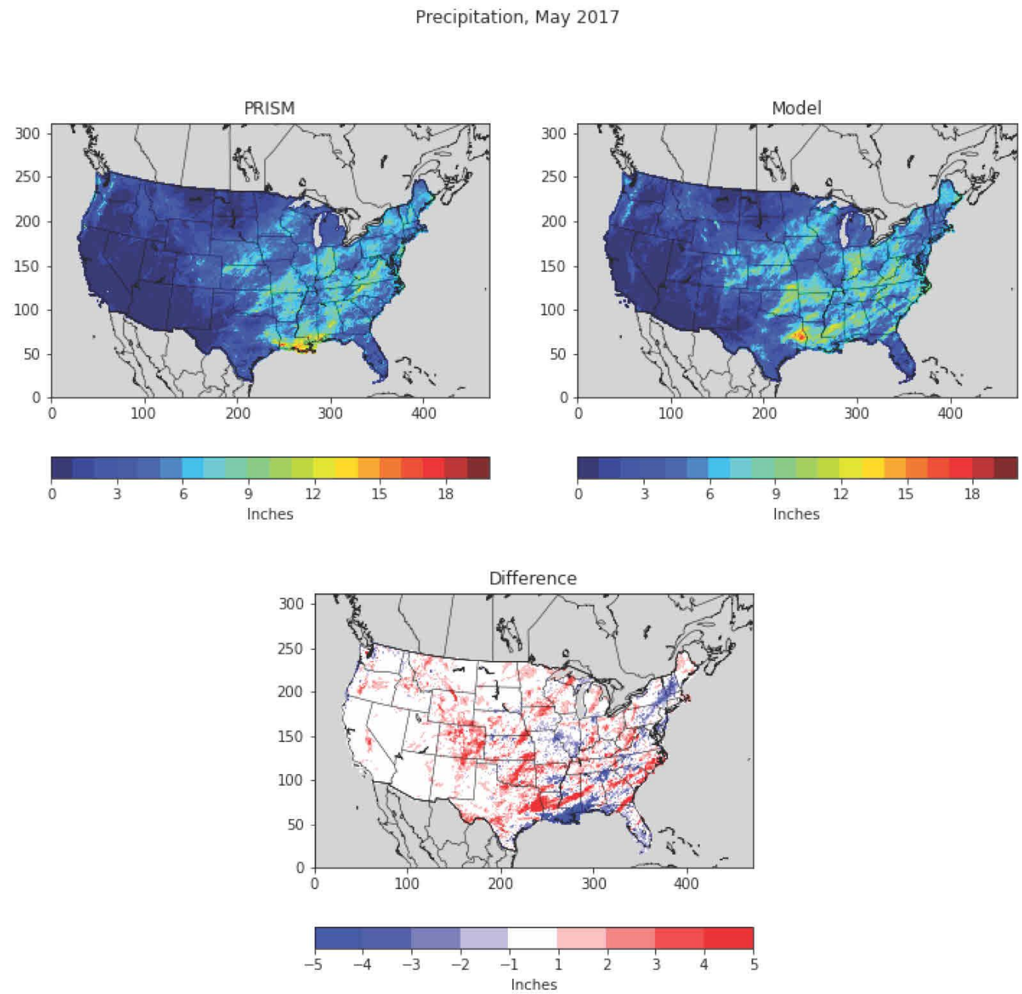

Figure 3.4.5. PRISM analysis (top left) and WRF (top right) estimated monthly total rainfall (in) and the difference (bottom) for May.

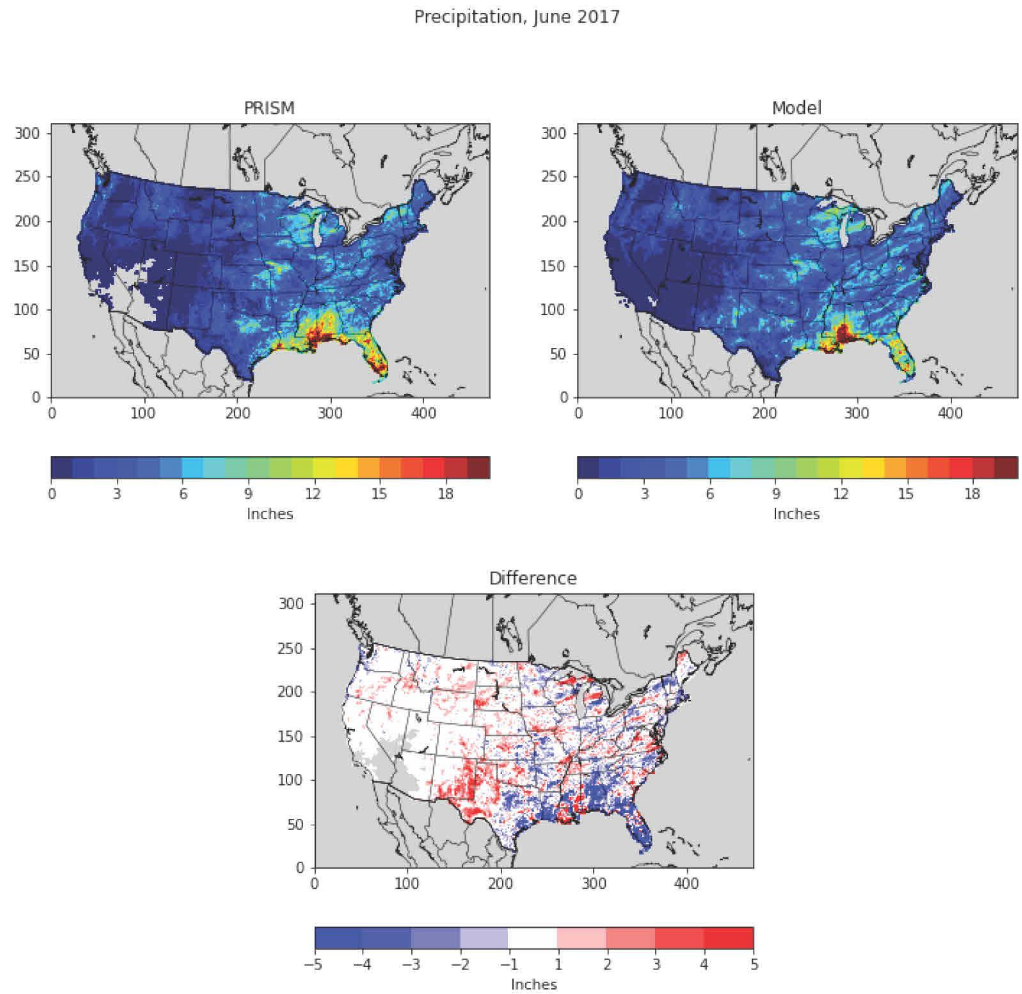

Figure 3.4.6. PRISM analysis (top left) and WRF (top right) estimated monthly total rainfall (in) and the difference (bottom) for June.

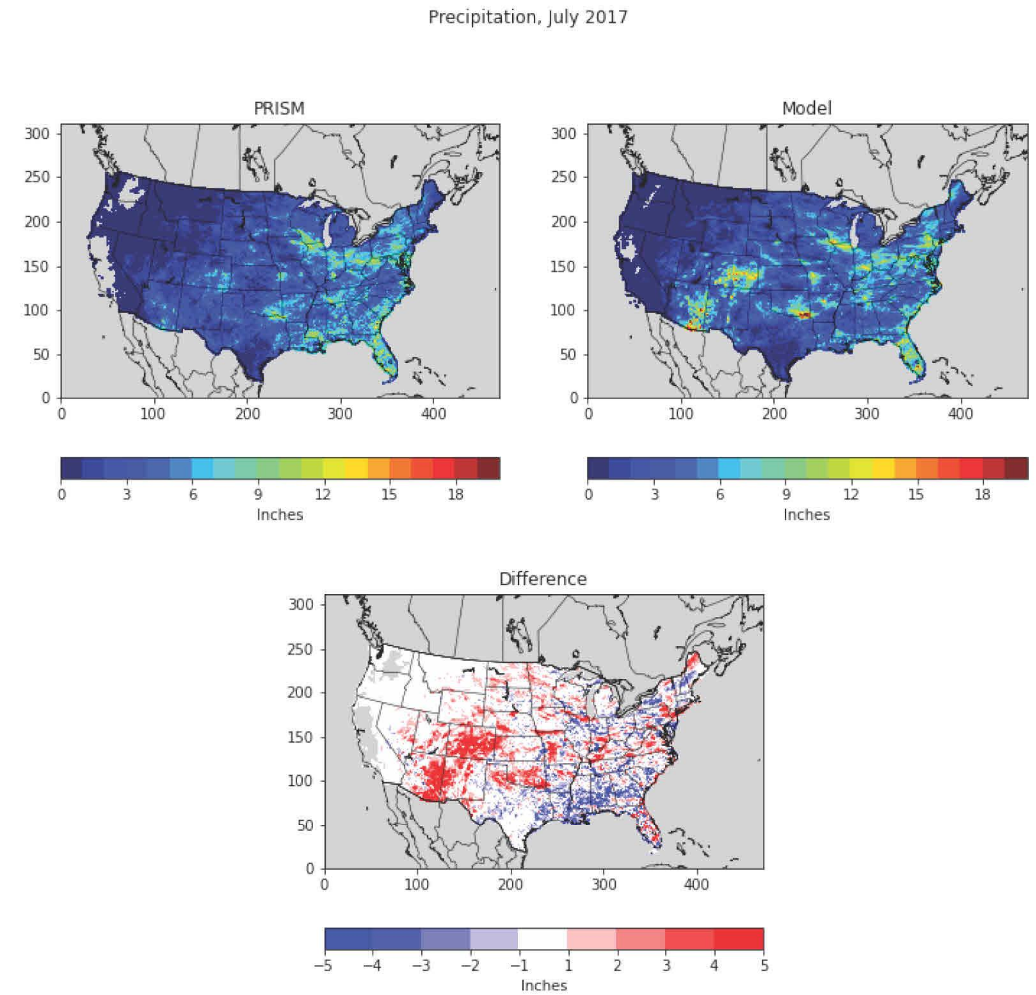

Figure 3.4.7. PRISM analysis (top left) and WRF (top right) estimated monthly total rainfall (in) and the difference (bottom) for July.

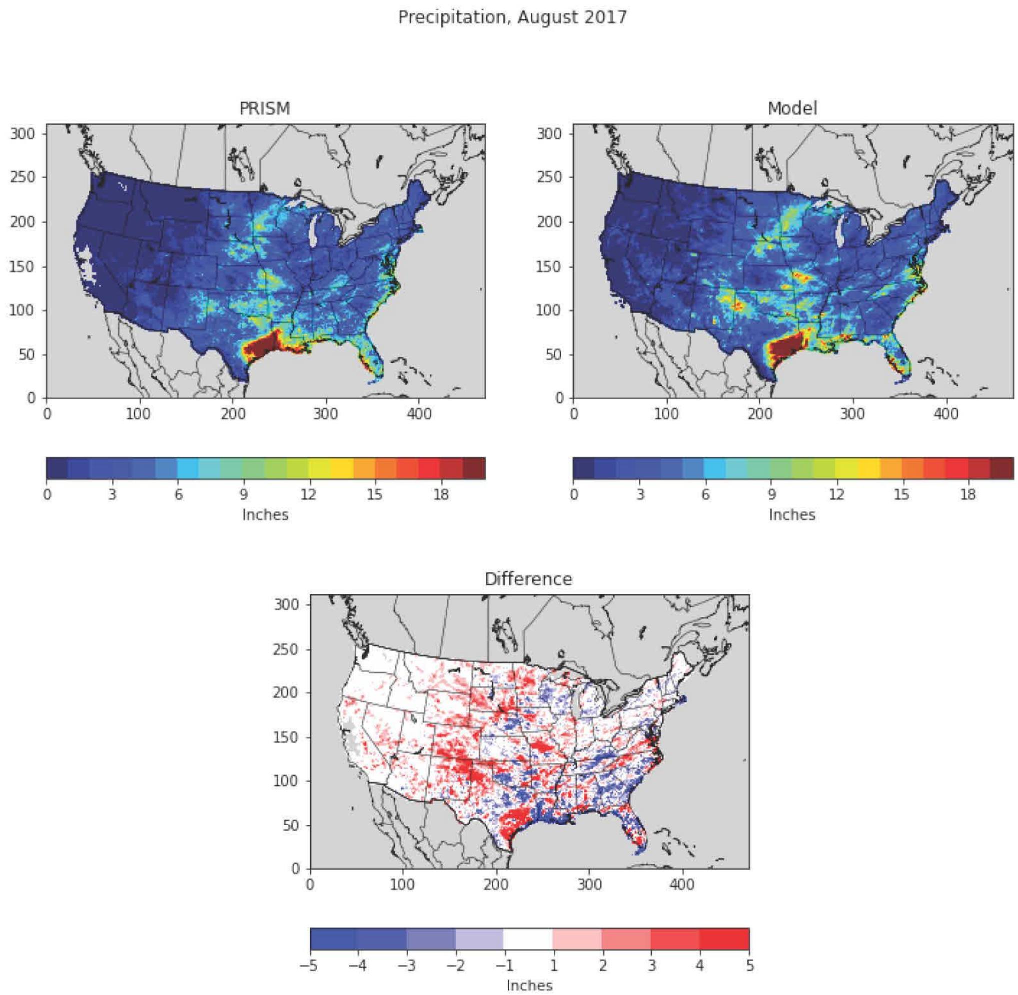

Figure 3.4.8. PRISM analysis (top left) and WRF (top right) estimated monthly total rainfall (in) and the difference (bottom) for August.

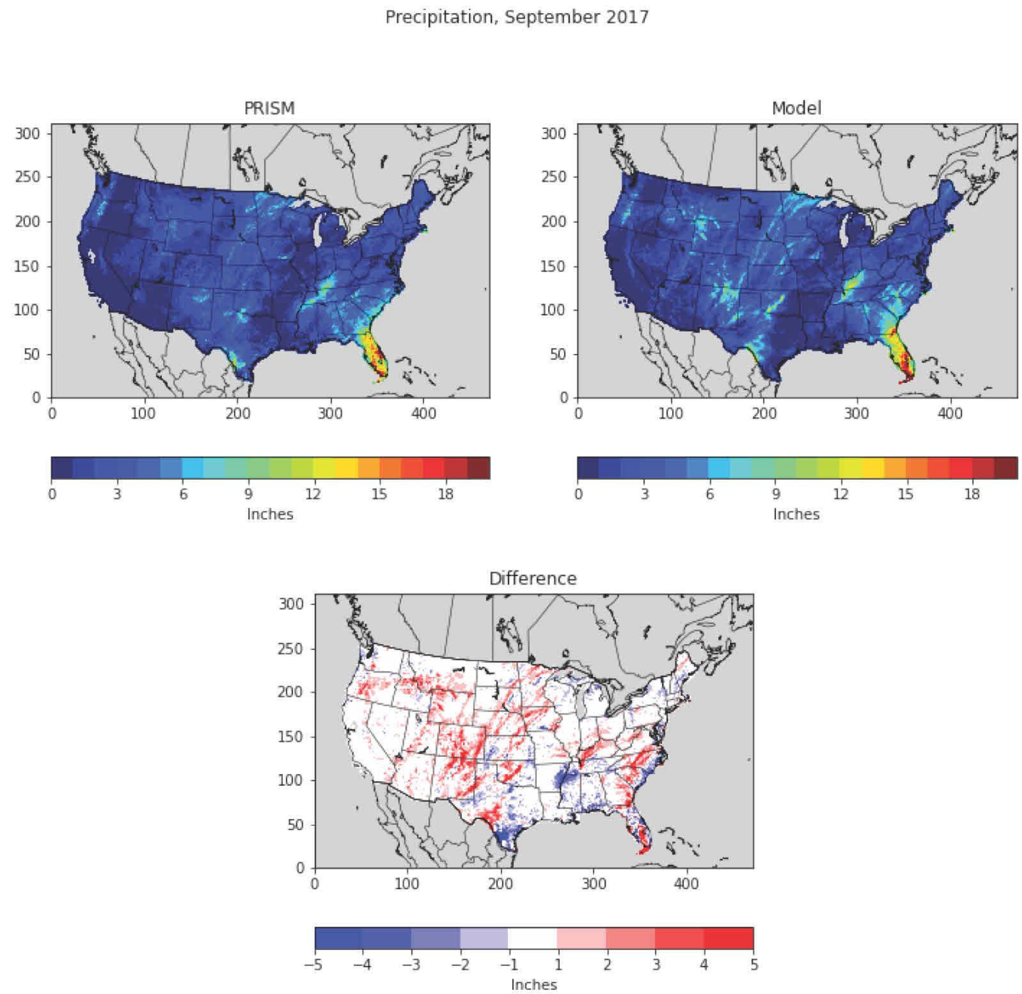

Figure 3.4.9. PRISM analysis (top left) and WRF (top right) estimated monthly total rainfall (in) and the difference (bottom) for September.

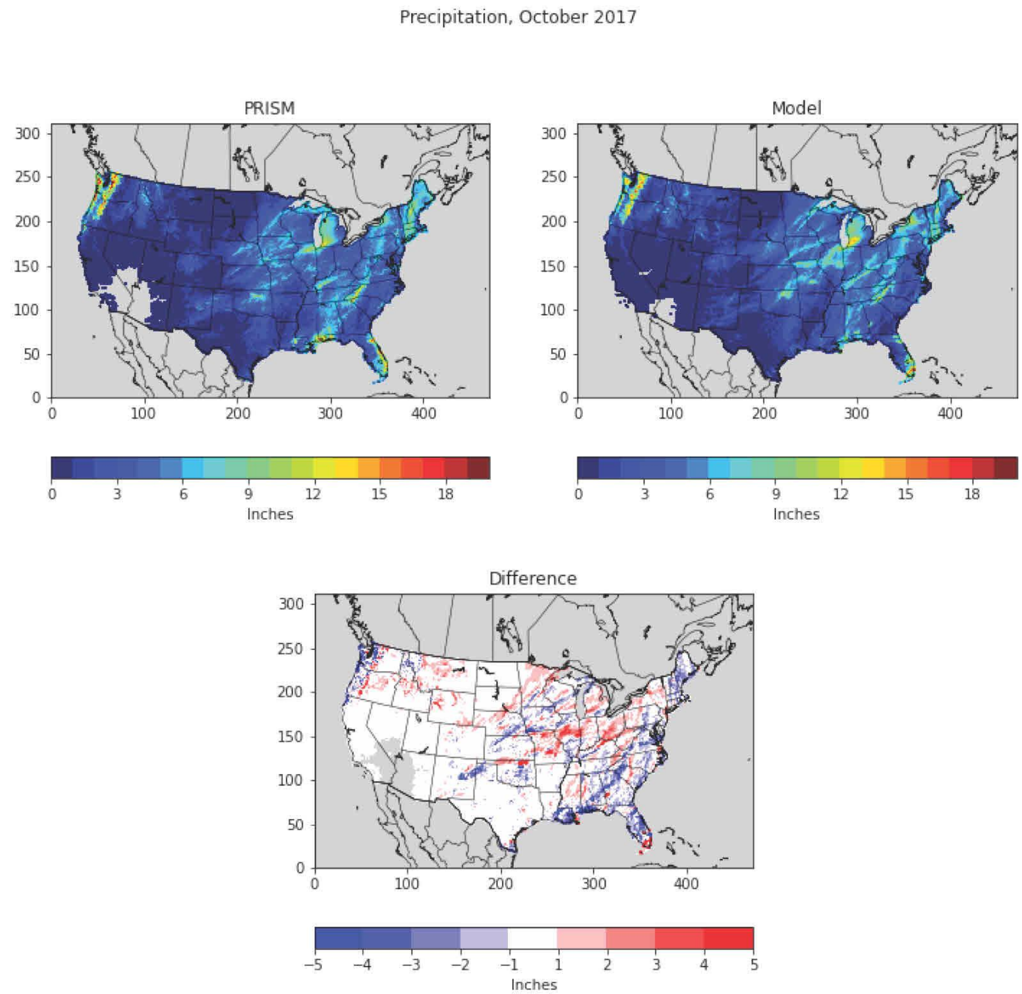

Figure 3.4.10. PRISM analysis (top left) and WRF (top right) estimated monthly total rainfall (in) and the difference (bottom) for October.

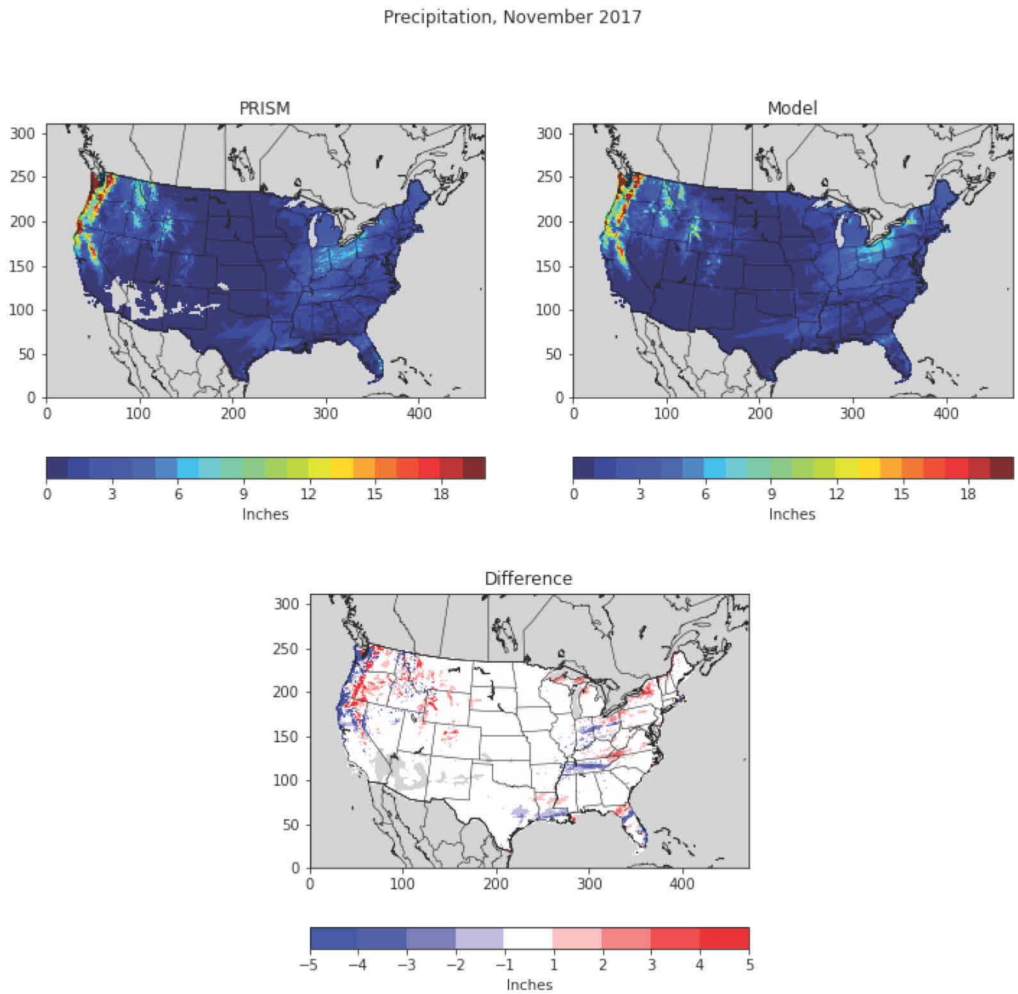

Figure 3.4.11. PRISM analysis (top left) and WRF (top right) estimated monthly total rainfall (in) and the difference (bottom) for November.

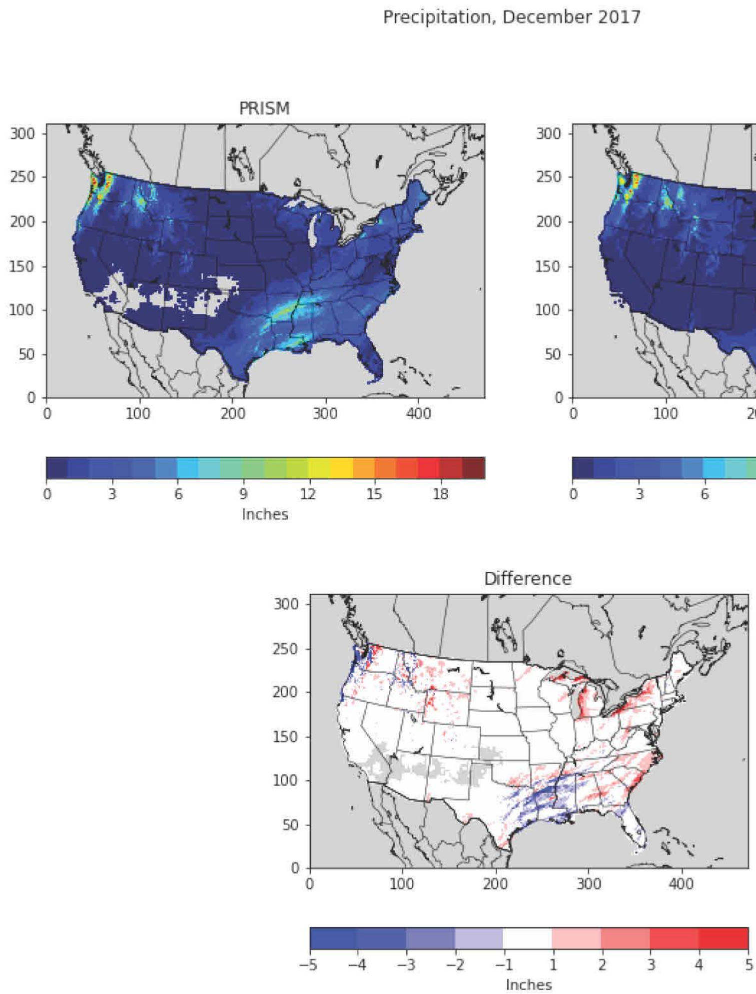

Figure 3.4.12. PRISM analysis (top left) and WRF (top right) estimated monthly total rainfall (in) and the difference (bottom) for December.

3.5 Solar Radiation

Photosynthetically activated radiation (PAR) is a fraction of shortwave downward radiation and is an important input for the biogenic emissions model for estimating isoprene (Carlton and Baker, 2011). Isoprene emissions are important for regional ozone chemistry and play a role in secondary organic aerosol formation. Radiation performance evaluation also gives an indirect assessment of how well the model captures cloud formation during daylight hours.

Shortwave downward radiation estimates are compared to surface-based measurements made at SURFRAD and SOLRAD network (Figure 3.5.1).

Overall, WRF has little bias in shortwave radiation predictions during the fall and winter months, but overpredicts slightly in general across most months. Biases tend to grow during the spring and peak in the summer, though the spread in overpredictions tends to be less than 50 W/m^2 on average, with a median bias close to zero.

More variability is noted on an hourly basis. WRF tends to overpredict shortwave radiation across all daytime hours. The median overprediction at the time of greatest incoming solar radiation is less than 50 W/m^2. A significant spread in the model biases is noted in the afternoon hours during peak radiation. These errors are likely attributable to the model being unable to accurately simulate cloud features at subgrid (<12km) scales.

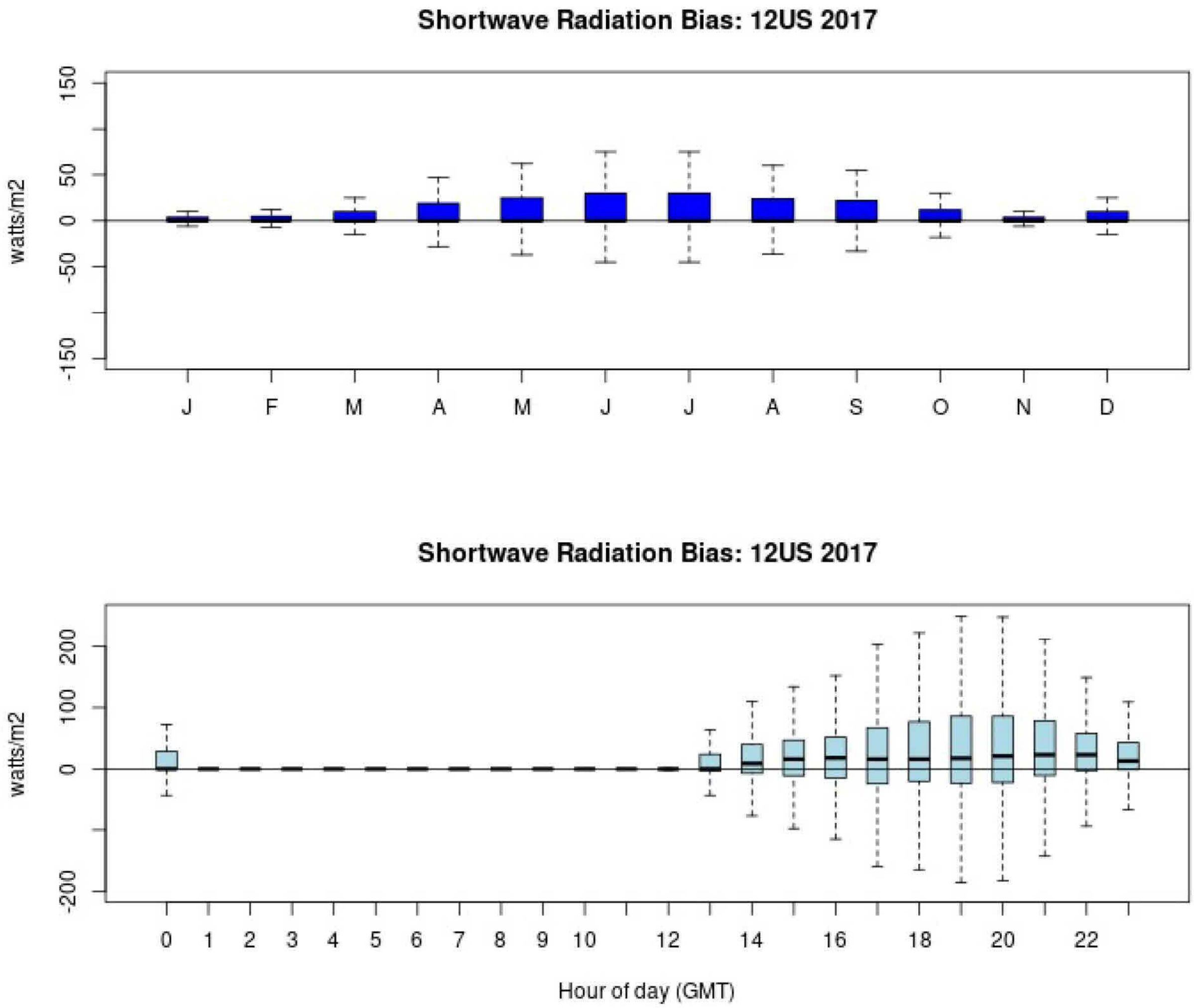

Figure 3.5.1. Distribution of hourly bias for shortwave radiation (W/m^2) by month (top) and by

4 CLIMATE REPRESENTATIVENESS OF 2017

Figures 4.1 and 4.2 show the divisional rankings for observed temperatures across the US for 2017. A climatic representation of the precipitation for 2017 is shown in Figures 4.3 and 4.4. We can use these plots to determine whether the conditions in a specific year are particularly anomalous. Additionally, we can make determinations of their suitability for use in photochemical modeling in terms of a specific year's conduciveness for photochemical production of secondary pollutants.

Temperatures in 2017 were above average to much above average across several months of the year, with record warmth observed in the central and eastern US during the late winter and early spring months. Normal to slightly below normal conditions were observed during the summer months for a large portion of the country, with much below average temperatures in late summer.

In general, 2017 was wetter than normal for most of the year, though below average precipitation was observed for the late Fall and Winter months.

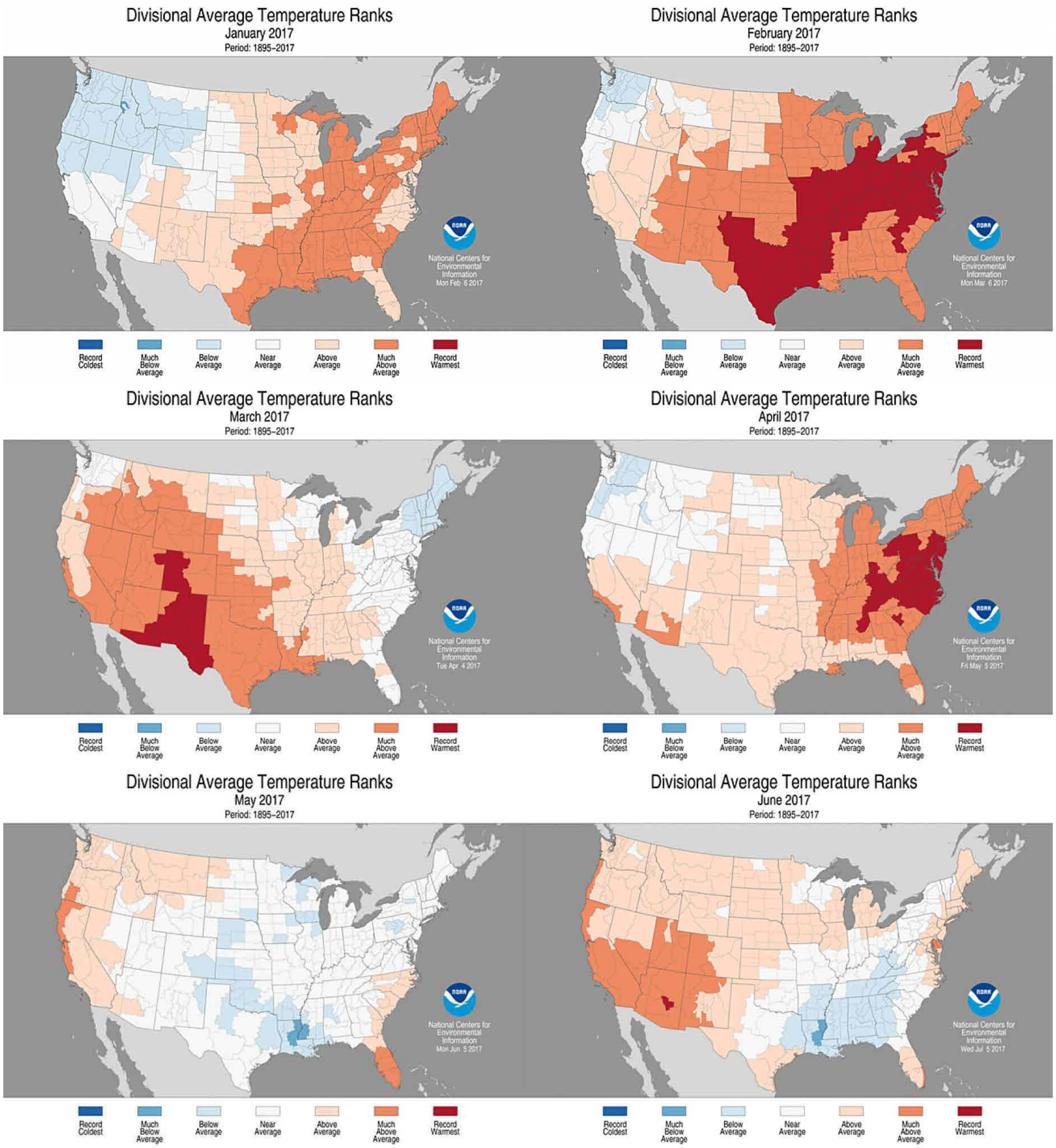

Figure 4.1 Climatic temperature rankings by climate division: January to June 2017. http://www.ncdc.noaa.gov/temp-and-precip/maps.php

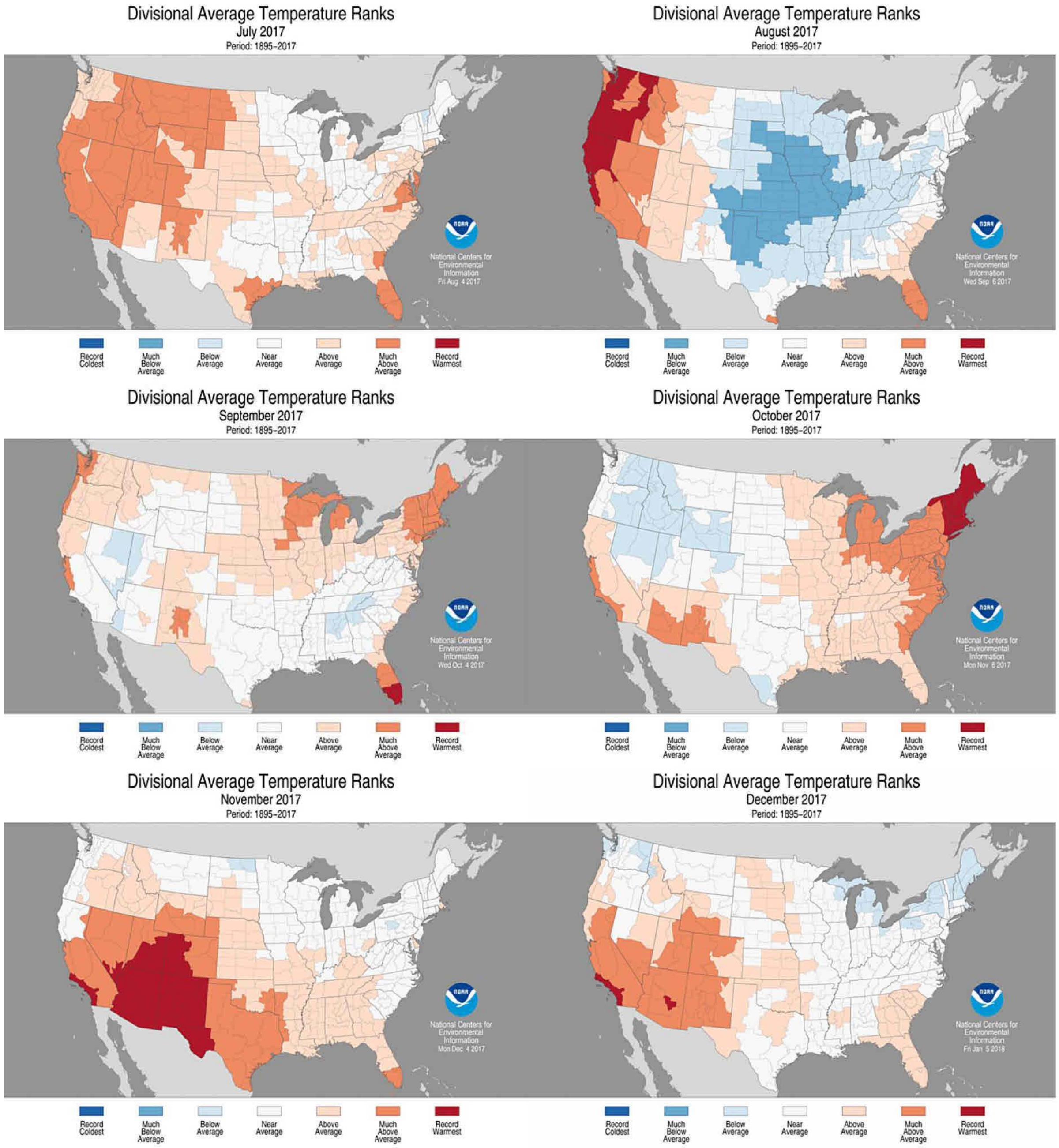

Figure 4.2 Climatic temperature rankings by climate division: July to December 2017. http://www.ncdc.noaa.gov/temp-and-precip/maps.php

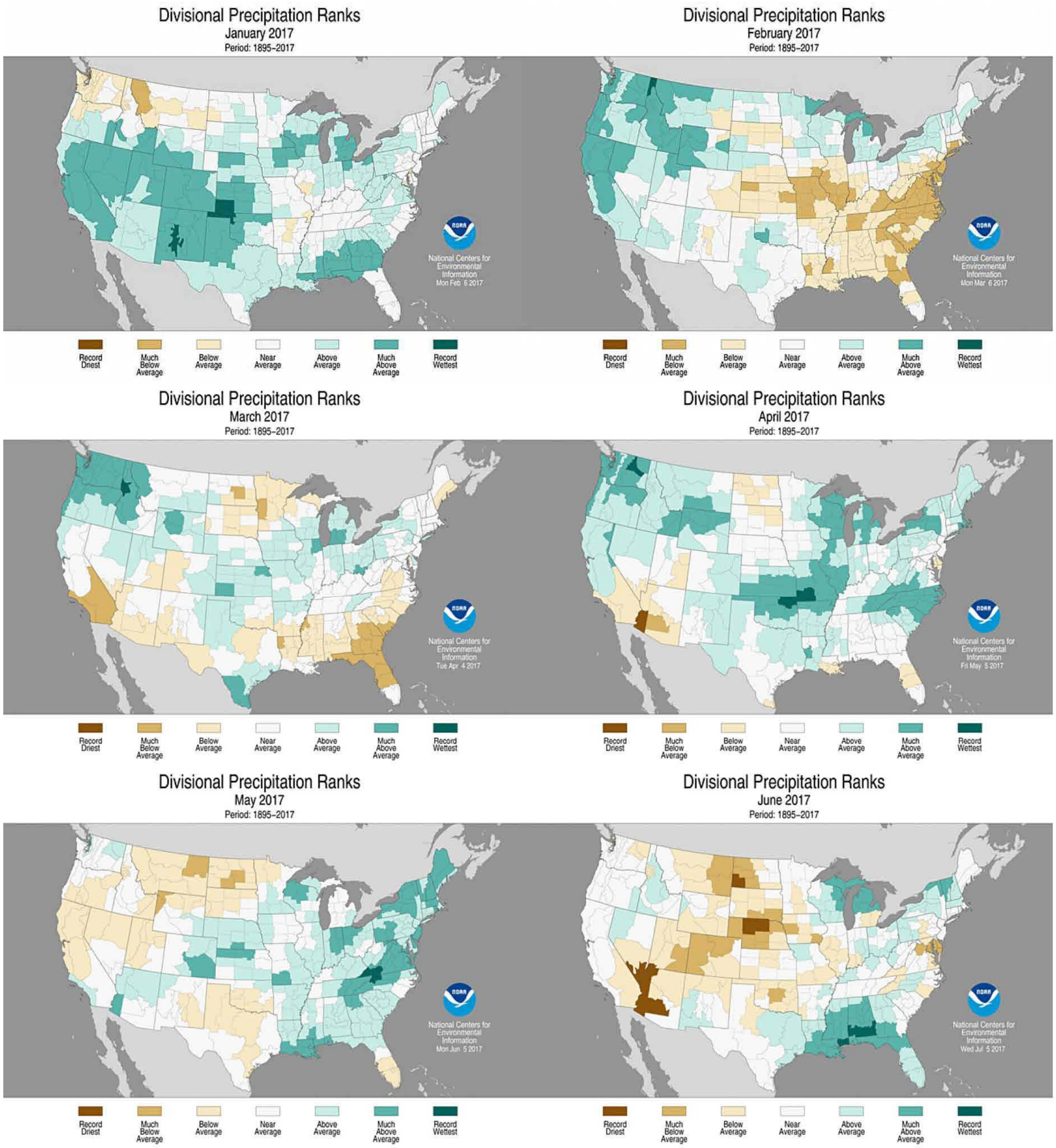

Figure 4.3 Climatic rainfall rankings by climate division: January to June 2017. http://www.ncdc.noaa.gov/temp-and-precip/maps.php

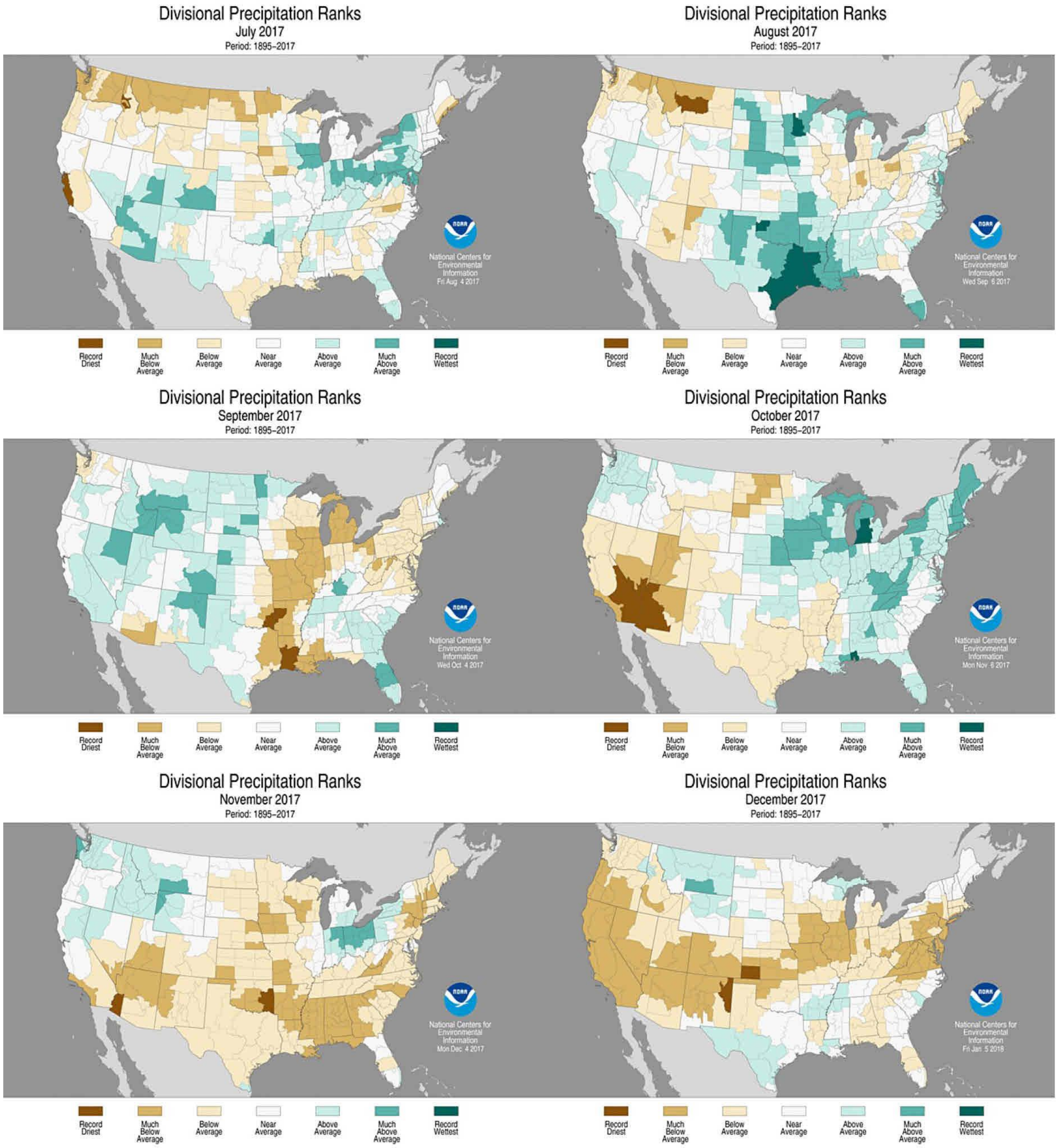

Figure 4.4 Climatic rainfall rankings by climate division: July to December 2017. https://www.ncdc.noaa.gov/sotc/

5 REFERENCES

Boylan, J.W., Russell, A.G., 2006. PM and light extinction model performance metrics, goals, and criteria for three-dimensional air quality models. Atmospheric Environment 40, 4946-4959.

Carlton, A.G., Baker, K.R., 2011. Photochemical Modeling of the Ozark Isoprene Volcano: MEGAN, BEIS, and Their Impacts on Air Quality Predictions. Environmental Science & Technology 45, 4438-4445.

Cooper, O.R., Stohl, A., Hubler, G., Hsie, E.Y., Parrish, D.D., Tuck, A.F., Kiladis, G.N., Oltmans, S.J., Johnson, B.J., Shapiro, M., Moody, J.L., Lefohn, A.S., 2005. Direct Transport of Midlatitude Stratospheric Ozone into the Lower Troposphere and Marine Boundary Layer of the Pacific Ocean. Journal of Geophysical Research – Atmospheres 110, D23310, doi:10.1029/2005JD005783.

ENVIRON, 2008. User's Guide Comprehensive Air Quality Model with Extensions. ENVIRON International Corporation, Novato.

Gilliam, R.C., Pleim, J.E., 2010. Performance Assessment of New Land Surface and Planetary Boundary Layer Physics in the WRF-ARW. Journal of Applied Meteorology and Climatology 49, 760-774.

Heath, Nicholas K., Pleim, J.E., Gilliam, R., Kang, D., 2016. A simple lightning assimilation technique for improving retrospective WRF simulations. Journal of Advances in Modeling Earth Systems. 8. 10.1002/2016MS000735.

Langford, A.O., Reid, S.J., 1998. Dissipation and Mixing of a Small-Scale Stratospheric Intrusion in the Upper Troposphere. Journal of Geophysical Research 103, 31265-31276.

Otte, T.L., Pleim, J.E., 2010. The Meteorology-Chemistry Interface Processor (MCIP) for the CMAQ modeling system: updates through MCIPv3.4.1. Geoscientific Model Development 3, 243-256.

Skamarock, W.C., Klemp, J.B., Dudhia, J., Gill, D.O., Barker, D.M., Duda, M.G., Huang, X., Wang, W., Powers, J.G., 2008. A Description of the Advanced Research WRF Version 3.

Stammer, D., F.J. Wentz, and C.L. Gentemann, 2003, Validation of Microwave Sea Surface Temperature Measurements for Climate Purposes, *J. Climate,* 16, 73-87.

United States Environmental Protection Agency	Office of Air Quality Planning and Standards Air Quality Assessment Division Research Triangle Park, NC	Publication No. EPA-454/R-22-006 September 2022